Synthesis of Novel Plant Oil Derivatives: Furan and Diels-Alder Reaction Products

Atanu Biswas*[1], Zengshe Liu[1], Janet L. Berfield[1], H. N. Cheng*[2]

[1]National Center for Agricultural Utilization Research, U.S. Department of Agriculture, Agricultural Research Service, 1815 N. University St., Peoria, IL 61604, USA

[2]Southern Regional Research Center, U.S. Department of Agriculture, Agricultural Research Service, 1100 Robert E. Lee Blvd., New Orleans, LA 70124, USA

atanu.biswas@ars.usda.gov; hn.cheng@ars.usda.gov

Abstract

Plant oils are useful sustainable raw materials for the development of new chemical products. In this work epoxidized soybean oil was treated with different acids, and variable amounts of furan structures were produced from the epoxidized linoleate moiety. From process studies, the highest yields of furan were obtained with fluorosulfonic and sulfuric acids. Using epoxidized methyl linoleate as a model compound, we obtained up to 14% furan with fluorosulfonic acid. The relationship between furan formation and ester hydrolysis was found to be a function of temperature and amount of acid used. In epoxidized soybean oil, up to about 7% of the furan structure was found. The furan moiety can undergo Diels-Alder reaction with maleimide and N-phenyl maleimide to form novel plant oil derivatives.

Keywords

Soybean Oil; Epoxidation; Fluorosulfonic Acid; Furan; Maleimide Derivative

Introduction

There has been a fair amount of interest in using plant oils as agriculturally based, sustainable, renewable, and environmentally friendly raw materials for the design and the production of specialty chemicals for various industrial applications (Biswas *et al.* 2008, Meier *et al.* 2007, Sharma and Kundu 2006, Biermann *et al.* 2000). Already numerous derivatives and polymers of plant oils have been made. Some materials have been successfully commercialized, including epoxidized soybean oil (Tayde *et al.* 2011, Petrovic *et al.* 2002), methyl soyate (methyl ester of soybean oil) (Knothe 2005, Srivastava and Prasad 2000), and vegetable oil lubricants (Ramadhas *et al.* 2004). These developments have been previously reviewed (Biswas *et al.* 2008, Meier *et al.* 2007, Sharma and Kundu 2006, Biermann *et al.* 2000). Despite these promising developments, new plant oil derivatives and new reaction processes involving sustainable raw materials are always welcome.

Recently furan-containing materials have found favor among people interested in renewable resources. Hydroxymethylfurfural (HMF) is derived from dehydration of certain sugars (Rosatella *et al.* 2011, van Putten *et al.* 2013) and is considered a platform chemical and a potential "carbon-neutral" feedstock for many specialty chemicals. Thus, alkoxymethylfurfurals, 2,5-furandicarboxylic acid, 5-hydroxymethylfuroic acid, bishydroxymethylfuran, and 2,5-dimethylfuran can be derived from HMF and potentially used in fuel or polymer applications (van Putten *et al.* 2013). Nonfuranic compounds that can be produced from HMF include levulinic acid, adipic acid, 5-hydroxy-4-keto-2-pentenoic acid, 1,6-hexanediol, caprolactam, and caprolactone (Rosatella *et al.* 2011, van Putten *et al.* 2013). Furan itself is known to be a good synthon for new reaction pathways, including Diels-Alder reactions (Kappe *et al.* 1997).

We have now found in this work a new reaction process whereby furan can be generated from plant oils. This requires the reaction of epoxidized linoleate moiety with an appropriate acid. Subsequently the furan adduct can be subjected to Diels-Alder reaction to form additional derivatives. The chemical structures have been identified, and quantification achieved through NMR studies. Whereas the reaction of an inorganic or Lewis acid with

2327-7246/15/02 028-8 © 2015 DEStech Publications, Inc.
doi:10.12783/ijast.2015.0302.01

epoxidized plant oils is previously known (Liu and Erhan 2010, Liu *et al.* 2009), the formation of furan structure from epoxidized soybean oil has not been reported, and the Diels-Alder derivatives are also not previously known. We have also carried out some process studies in order to understand the effects of reaction parameters on the formation of furan and Diels-Alder products.

Materials and Methods

Materials

Fluorosulfonic acid (triple distilled), trifluoroacetic acid, methyl esters of oleic acid and linoleic acid were acquired from Sigma Aldrich (Milwaukee, Wisconsin). Perchloric acid (70%) came from Fisher Scientific (Pittsburgh, Pennsylvania). Sulfuric acid came from J.T. Baker (Phillipsburg, New Jersey), and p-toluene sulfonic acid from MCB Reagents (Cincinnati, Ohio). Soybean oil came from a local supermarket. Arkema Inc. (King of Prussia, Pennsylvania) supplied the epoxidized soybean oil (Vikoflex® 7170). Deuterochloroform came from Cambridge Isotope Laboratories, Inc., Andover, Massachusetts.

Furan Formation

A typical procedure involved the addition of 1 g epoxidized methyl linoleate (EMLO) or ESO and 2-5 mL ethyl acetate in a glass vial with stir bar, screw cap with septum. Into the vial 5-80 mg of fluorosulfonic acid was added. The vial was placed in a React-Therm™ reactor set at 25-77ºC for 4-24 hours with the reaction under nitrogen and stirring. As a precaution, an extra needle in the cap was inserted to prevent pressure buildup. At the completion of the reaction, water was added to the vial, mixed, and decanted off. Sodium bicarbonate solution (5%) was then added, mixed, and decanted off. The product was washed twice with deionized water and then dried in vacuo at 40ºC. In this procedure recovery of EMLO or ESO derivatives was essentially quantitative, varying from 92-99%.

Diels-Alder Reaction

In the two-step process, Diels-Alder reaction was carried out typically with 1 g EMLO-furan or ESO-furan derivative. It was mixed with 0.1 – 0.3 g maleimide or N-phenyl maleimide and 3-4 g of ethyl acetate. The reaction mixture was heated at 60-65ºC for 24 hours. After reaction, the product was washed with water and stripped of the solvent with a rotary evaporator.

In the one-step process, both the furan formation and Diels-Alder reaction were carried out in the same pot. Typically 1 g of EMLO or ESO, 0.05-0.3 g of maleimide or N-phenyl maleimide, 20 mg fluorosulfonic acid, and 2 g ethyl acetate were mixed together and heated in a React-Therm™ at 60ºC for 4-16 hours. At the completion of the reaction, the reaction product was washed with water, 5% sodium bicarbonate solution, and water again before the solvent was stripped off with a rotary evaporator. In this procedure most of the Diels-Alder derivatives were recovered except for loss due to handling and transfer.

NMR Analysis

NMR spectra were acquired on a Bruker DRX 400 spectrometer (Karlsruhe, Germany). The NMR solvent was $CDCl_3$. The ^{1}H and ^{13}C shift reference was tetramethylsilane (at 0 ppm). Standard operating conditions were used with 30^{o} pulse angle and 3 seconds between pulses.

The ^{13}C NMR spectra of fluorosulfonic acid-generated furan products from EMLO and ESO are shown in FIGURE 1. The spectral assignments were achieved via shift additivity rules (Cheng and Kasehagen 1994, Cheng and Bennett 1991) and from ^{13}C predicted shifts from compounds given in the literature (MestReNova 2014). The amounts of different species present were estimated by using the area of the 22.3 ppm peak (ω-2 in the fatty acid) as reference and taking the areas of the peaks for other species. From ^{13}C NMR spectrum of the EMLO product (FIGURE 1, upper plot), the furan f_1 peak occurs at ~ 155 ppm and furan f_2 peak at ~ 115 ppm. Because the f_1 carbon has no attached hydrogen, its peak area is reduced under the NMR experimental conditions used, and only the area of f_2 peak is used for quantification. The ^{13}C NMR peak at 53 ppm corresponds to the methoxy carbon. The

area of the methoxy peak becomes smaller when hydrolysis of the methyl ester occurs; thus from the methoxy peak area, the degree of ester hydrolysis can be estimated. Likewise, the ^{13}C NMR spectrum of the ESO product is given in FIGURE 1, lower plot. As in the case of EMLO, the furan f_1 and f_2 peaks can be clearly observed in the ^{13}C NMR spectrum. In addition, the glycerate ester peaks can be seen at ~ 63 and 68 ppm; from the area of the glycerate peaks, the amount of hydrolysis of the glycerate ester can be estimated. Note that in the spectra there were many peaks in the 72-86 ppm range; these corresponded to the polymers of EMLO or ESO (Liu and Erhan 2010, Liu *et al.* 2009), which were also generated by the action of the fluorosulfonic acid.

The ^{13}C NMR spectra of the furan-maleimide Diels-Alder products derived from EMLO and ESO are shown in FIGURE 2. The spectral assignments were achieved via shift additivity rules (Cheng and Kasehagen 1994, Cheng and Bennett 1991) and from the ^{13}C shifts of model reactions carried out in this work involving the Diels-Alder reactions of 1,4-dimethylfuran and maleimide (^{13}C shifts found at 177, 141, 87, 54, and 16 ppm), and 1,4-dimethylfuran and N-phenylmaleimide (^{13}C shift found at 174, 141, 131, 129, 128, 126, 88, 53, 16 ppm). The amounts of different species present were estimated by using the area of the 22.3 ppm peak (ω-2 in the fatty acid) as reference and taking the areas of the peaks for other species. From ^{13}C NMR spectrum of the Diels-Alder product of EMLO furan and maleimide (FIGURE 2, upper plot), the furan peaks and methoxy peaks can be seen as in FIGURE 1. In addition, the Diels-Alder product can be clearly observed (d_1, d_2, d_3, and d_4) and quantified. Likewise, the ^{13}C NMR spectrum of the Diels-Alder product of ESO furan and maleimide is given in FIGURE 2, lower plot. As in FIGURE 1, the furan and glycerate peaks can be clearly observed in the spectrum; moreover, the Diels-Alder products can be observed (d_1, d_2, d_3, and d_4) and quantified. Note that in the spectra there were many peaks in the 72-86 ppm range; these corresponded to the polymers of EMLO or ESO (Liu and Erhan 2010, Liu *et al.* 2009), which were also generated by the action of the fluorosulfonic acid.

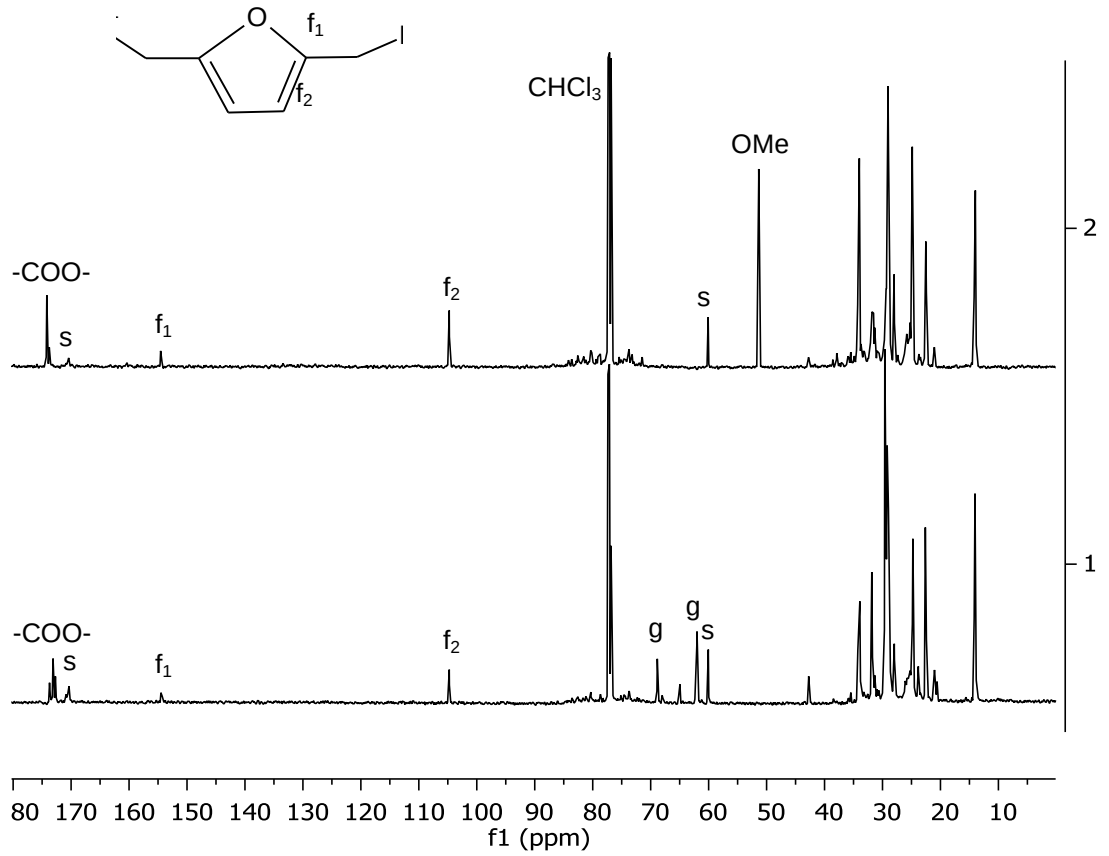

FIGURE 1. ^{13}C NMR SPECTRA OF SAMPLE 8 (FURAN DERIVATIVE FROM EMLO), UPPER SPECTRUM, AND SAMPLE 19 (FURAN DERIVATIVE FROM ESO), LOWER SPECTRUM; F = FURAN, G = GLYCERATE, S = RESIDUAL SOLVENT (ETHYL ACETATE)

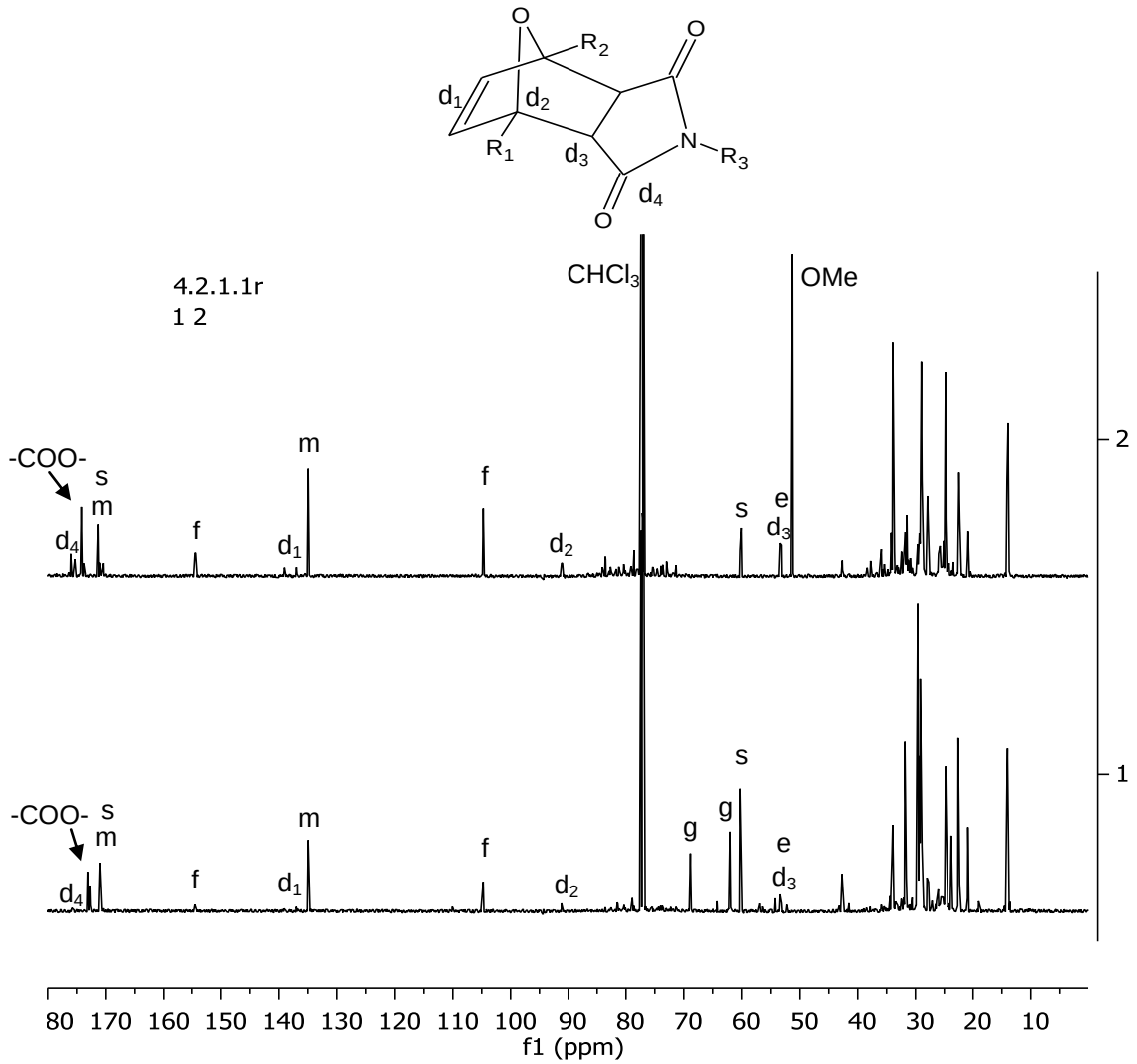

FIGURE 2. ^{13}C NMR SPECTRA OF SAMPLE 29 (DIELS-ALDER PRODUCT FROM FURAN-MALEIMIDE DERIVED FROM EMLO), UPPER SPECTRUM, AND SAMPLE 30 (DIELS-ALDER PRODUCT FROM ESO), LOWER SPECTRUM; F = FURAN, D = DIELS-ALDER PRODUCT, G = GLYCERATE, E = RESIDUAL EPOXIDE, M = RESIDUAL MALEIMIDE, S = RESIDUAL SOLVENT (ETHYL ACETATE)

Results and Discussion

Epoxidization of methyl linoleate and soybean oil was achieved in the presence of hydrogen peroxide and perbenzoic acid (La Scala and Wool 2002, Doll and Erhan 2005). ESO was also purchased commercially. The NMR spectra indicate that the conversion of olefins to epoxides was almost quantitative in these samples.

Furan Formation

This work was initiated by our finding that the reaction of a strong acid with the diepoxide of methyl linoleate produced the furan structure, where R^1, R^2 correspond to the fatty chain residue.

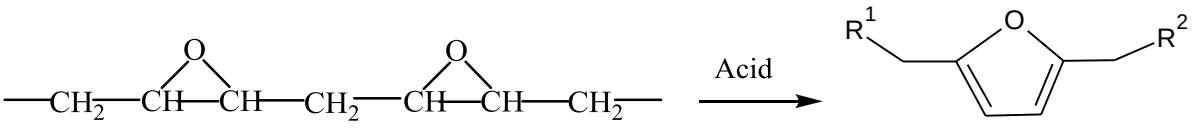

A systematic study was then made to optimize this reaction. First, five acids were selected for the reactions with epoxidized methyl linoleate (EMLO): fluorosulfonic acid, perchloric acid, sulfuric acid, p-toluenesulfonic acid, and trifluoroacetic acid. In each case the same amount of acid was used and the reaction was conducted at 80ºC. Analysis was carried out by ^{13}C NMR, as delineated in the Experimental Section. The quantitative results are summarized in Table 1 (samples 1-5). Under the reaction conditions used, it is clear that fluorosulfonic and sulfuric

acid gave the highest levels of furan. Perchloric acid also produced some furan, but the extent of ester hydrolysis was high (86%). The other two acids, p-toluenesulfonic acid and trifluoroacetic acid, did not produce any furan at all. Moreover, varying amounts of hydrolysis of the methyl ester was found in all the samples.

The perchloric acid used contained about 30% water. It was suspected that the water present caused the high level of ester hydrolysis. To prove this hypothesis, we carried out the same reaction with fluorosulfonic acid, except with two levels of water added (Table 1, samples 6 and 7). Indeed, the data indicate that with the presence of water the ester hydrolysis levels increased and the furan levels were suppressed.

We next examined the role of solvent. Five solvents were used for the reaction with 15 mg fluorosulfonic acid: ethyl acetate, chloroform, toluene, heptanes, and methylene chloride. In each case, the reaction mixture of EMLO, fluorosulfonic acid and solvent were stirred vigorously during heating. As it turned out, all solvents used gave roughly the same levels of furan and ester hydrolysis, 23-30%, with the exception of methylene chloride (Table 2). In the case of methylene chloride, the lower ester hydrolysis was due to the lower temperature used (*vide infra*). In view of the ready solubility of fluorosulfonic acid in ethyl acetate, we preferred to use ethyl acetate as the solvent in the rest of this work.

TABLE 1. EFFECTS OF DIFFERENT ACIDS ON ESTER HYDROLYSIS AND FURAN FORMATION, ALL RUNS DONE WITH 1 GRAM EMLO IN ETHYL ACETATE SOLVENT AT 77°C

No	sample	condition	reaction time (h)	ester hydrolysis (%)	furan (%)
1	EMLO	fluorosulfonic, 20 mg	24	32	12
2	EMLO	perchloric, 20 mg	16	86	5.5
3	EMLO	sulfuric, 20 mg	16	38	11.5
4	EMLO	p-toluenesulfonic, 20 mg	16	4	0
5	EMLO	trifluoroacetic, 20 mg	16	4	0
6	EMLO	fluorosulfonic, 20 mg + water 25 ul	16	86	4
7	EMLO	fluorosulfonic, 20 mg + water 50 ul	16	96	5

TABLE 2. EFFECTS OF DIFFERENT SOLVENTS ON HYDROLYSIS AND FURAN FORMATION, ALL RUNS DONE WITH 1 GRAM EMLO AT 24 HOURS

No	sample	solvent	condition	reaction temp (°C)	ester hydrolysis %	furan %
8	EMLO	EtAc	fluorosulfonic, 15 mg	77	30	12
9	EMLO	$CHCl_3$	fluorosulfonic, 15 mg	61	25	13.5
10	EMLO	Toluene	fluorosulfonic, 15 mg	80	23	12.5
11	EMLO	Heptane	fluorosulfonic, 15 mg	80	24	13.5
12	EMLO	CH_2Cl_2	fluorosulfonic, 15 mg	40	13	14

TABLE 3. EFFECTS OF DIFFERENT LEVELS OF FLUOROSULFONIC ACID AND REACTION TEMPERATURE ON ESTER HYDROLYSIS AND FURAN FORMATION, ALL RUNS DONE WITH 1 GRAM EMLO AT 24 HOURS

No	sample	condition	reaction temp (°C)	ester hydrolysis (%)	furan (%)
8	EMLO	fluorosulfonic, 15 mg, 2g EtAc	77	30	12
13	EMLO	fluorosulfonic, 15 mg, 2g EtAc	25	17	14
14	EMLO	fluorosulfonic, 10 mg, 2g EtAc	25	6	7
15	EMLO	fluorosulfonic, 5 mg, 2g EtAc	25	5	3.5
16	EMLO	fluorosulfonic, 2.5 mg, 2g EtAc	25	2	3

TABLE 4. EFFECTS OF DIFFERENT LEVELS OF FLUOROSULFONIC ACID, REACTION TIME, AND REACTION TEMPERATURE ON ESTER HYDROLYSIS AND FURAN FORMATION, ALL RUNS DONE WITH 1 GRAM ESO

No	sample	condition	reaction temp (°C)	reaction time (h)	ester hydrolysis (%)	furan (%)
17	ESO	fluorosulfonic, 5 mg, 2g EtAc	60	16	8	3
18	ESO	fluorosulfonic, 10 mg, 2g EtAc	60	16	18	6
19	ESO	fluorosulfonic, 20 mg, 2g EtAc	60	16	35	6
20	ESO	fluorosulfonic, 50 mg, 2g EtAc	60	16	49	7
21	ESO	fluorosulfonic, 10 mg, 2g EtAc	60	1 hr	16	4.5
22	ESO	fluorosulfonic, 10 mg, 2g EtAc	60	2 hrs	22	4.5
23	ESO	fluorosulfonic, 10 mg, 2g EtAc	60	12 hrs	23	4.5
24	ESO	fluorosulfonic, 10 mg, 2g EtAc	25	24	5	5
25	ESO	fluorosulfonic, 20 mg, 2g EtAc	25	24	9	5

TABLE 5. DIELS-ALDER (DA) REACTION OF FURAN PRODUCTS DERIVED FROM EMLO AND ESO. ALL REACTIONS DONE WITH 1 GRAM STARTING MATERIALS

No	sample	DA mode	condition	Reaction temp (ºC)	reaction time (h)	hydrolysis (%)	furan (%)	DA product (%)
8	EMLO	none	fluorosulfonic acid, 15 mg	60-65	0	30	12	0
26	8	two-step	0.1g MA	60-65	24	33	7	1
27	8	two-step	0.2g MA	60-65	24	33	5	3
28	8	two-step	0.2g PMA	60-65	24	33	2	3
29	EMLO	one-step	fluorosulfonic acid, 20 mg + 0.1g MA	60-65	16	19	10.5	3.5
30	ESO	one-step	fluorosulfonic acid, 20 mg + 0.1g MA	50	24	9	2	3
31	EMLO	one-step	fluorosulfonic acid, 20 mg + 0.1g MA	35	16	7	4	7
32	ESO	one-step	fluorosulfonic acid, 20 mg + 0.1g MA	35	24	5	4	3

We also examined the effects of reaction temperature and acid level. To check the effect of temperature, we carried out a run using 15 mg of fluorosulfonic acid at 25ºC (Table 3, sample 13). In this case, the amount of ester hydrolysis was almost reduced to one-half, while the furan level increased slightly (cf. samples 8 and 13). In addition, the level of fluorosulfonic acid was decreased from 15 mg to 2.5 mg, while keeping all other reaction parameters the same (Table 3, samples 14, 15, 16). In this case, the hydrolysis and the furan levels steadily decreased with decrease in acid level. At lower acid levels, some unreacted epoxide could be observed. Thus, there appears to be an optimal temperature and acid level that can maximize furan concentration and minimize ester hydrolysis.

Whereas epoxidized methyl linoleate is a useful material, it is even more interesting to study the reaction of the fluorosulfonic acid with epoxidized soybean oil (ESO). The reaction of ESO with different levels of fluorosulfonic acid (from 5 mg to 50 mg) is shown Table 4 (samples 17-20). Note that as the acid level increased, ester hydrolysis also increased; the furan level was lower at low acid level, but increased steadily with higher acid levels. The trend was consistent with what we observed for EMLO (Table 3). The reaction with 10 mg fluorosulfonic acid was also studied at different reaction times (Table 4, samples 21, 22, 23). In this case, the effect of reaction time appeared to be relatively small. The reaction seemed to occur quickly and was completed after 2 hours. Finally, the reaction of fluorosulfonic acid with ESO was studied at a lower temperature, 25ºC (Table 4, samples 24, 25). Relative to the 60ºC reaction, the ester hydrolysis decreased by one-half at 25ºC, whereas the furan level stayed about the same. This trend was similar to that found for EMLO (Table 3).

From the foregoing results, it seems that we can produce up to 10-14% furan in EMLO and about 5% furan in ESO under the reaction conditions studied thus far.

Diels-Alder Reactions

The ability to produce furan functionality in soybean oil and methyl linoleate systems provides an opportunity to derivatize the furan. One possible derivatization is the Diels-Alder reaction. As illustration, two compounds were chosen for this study: maleimide (MA) and N-phenyl maleimide (PMA).

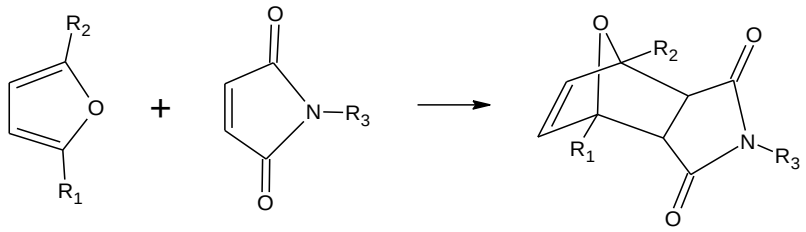

where R_1 and R_2 denote the two parts of the linoleic moiety adjacent to the furan ring, and R_3 is H or phenyl for MA or PMA, respectively. We started with a sample of furan product (sample 8) derived from EMLO; this sample contained 12% furan. Diels-Alder reaction was carried out in ethyl acetate at 60-65ºC for 24 hours. ^{13}C NMR analysis was used to identify and to quantify the reaction product as described in the Experimental Section. At 0.1

g and 0.2 g MA, about 1 and 3% Diels-Alder product was observed, respectively (Table 5, samples 26, 27). Likewise, at 0.2 g PMA, about 3% Diels-Alder product was observed (Table 5, sample 28). Note that the furan level also decreased as Diels-Alder products were formed, but the sum of furan and Diels-Alder product levels was less than the starting furan level, suggesting that some byproducts (as yet unidentified) were also formed.

We then sought to do the furan formation and Diels-Alder reaction in one step. Within the same reaction vessel, we placed EMLO, fluorosulfonic acid, maleimide, and ethyl acetate solvent. The reaction mixture was heated at 60ºC for 16 hours. Analysis was again carried out by ^{13}C NMR. The results (Table 5, sample 29; also FIGURE 2, upper plot) indicated 3.5% Diels-Alder product was produced. The ester hydrolysis level was reduced perhaps due to the buffering action of maleimide. We also attempted the one-step reaction on ESO at 50ºC. The result (Table 5, sample 30; also FIGURE 2, lower plot) also seemed satisfactory, with about 2% furan and 3% Diels-Alder product formed.

As an additional iteration, we lowered the reaction temperature to 35ºC. The results for EMLO (Table 5, sample 31) are better, with about 4% furan and 7% Diels-Alder product formed. For ESO, the results at 35ºC (Table 5, sample 32) are slight improvements over those at 50ºC, with a higher level of furan (4%), the same amount of Diels-Alder product (3%), and a lower level of ester hydrolysis (5%). It is possible that even further improvements may be possible with additional process studies.

Potential Applications

Thus, through the use of an acid, it is possible to produce the furan functionality from epoxidized methyl linoleate and epoxidized soybean oil. The furan functionality is a useful synthon for further derivatization reactions. As proof of concept, the Diels-Alder reaction between the functionality generated in this work has been demonstrated for maleimide and N-phenyl maleimide. Other Diels-Alder derivatives can be likewise devised. For example, the maleimide derivative with p-aminobenzoic acid (PABA) may be of interest. The PABA-maleimide compound can be adducted onto the soybean oil-furan with the Diels-Alder reaction. Since PABA is a well-known active ingredient in sunscreens, this Diels-Alder adduct of soybean oil can probably be used for the sunscreen application. As another example, nicotine is a natural insecticide; it can be grafted onto maleimide and attached to soybean oil-furan through Diels-Alder reaction to produce a potentially active ingredient for insect repellent on skin. For these types of applications, a high level of the Diels-Alder derivative in triglycerides or fatty acid methyl esters may not be necessary. Application work involving furan and Diels-Alder reactions may be contemplated in the future.

Conclusion

In contrast to petroleum-based raw materials, plant oils are considered desirable alternatives for the syntheses of selected specialty chemicals. The present data give one example of how the furan moiety can be derived from soybean oil. In the process studies thus far, 10-14% furan can be produced in epoxidized methyl linoleate and about 5% furan in epoxidized soybean oil. This furan functionality can be further derivatized to generate new products from plant oils. As proof of principle, the Diels-Alder products of furan-maleimide and furan-N-phenyl maleimide have been synthesized. Since the Diels-Alder chemistry of furan is rich with structural possibilities (Kappe *et al.* 1997), potentially a family of new structures can be made based on the furan produced from triglycerides and fatty acid methyl esters.

ACKNOWLEDGEMENTS

Thanks are due to Karl Vermillion for the recording the NMR spectra. Mention of trade names or commercial products in this publication is solely for the purpose of providing specific information and does not imply recommendation or endorsement by the U.S. Department of Agriculture. USDA is an equal opportunity provider and employer.

REFERENCES

[1] Biermann, U., Friedt, W., Lang, S., Lühs, W., Machmüller, G., Metzger, J.O., Rüsch gen. Klaas, M., Schäfer, H.J. and Schneider, M.P. "New syntheses with oils and fats as renewable raw materials for the chemical industry."

Angew. Chem. Int. Ed. 39, 2206-2224, 2000.

[2] Biswas, A., Sharma, B.K., Willett, J.L., Erhan, S.Z., and Cheng, H.N. "Soybean oil as a renewable feedstock for nitrogen-containing derivatives." Energy Environ. Sci. 1, 639-644, 2008.

[3] Cheng, H. N. and Bennett, M. A. "Trends in ^{13}C NMR shifts and computer aided shift prediction." Anal. Chim. Acta 242, 43-56, 1991.

[4] Cheng, H. N. and Kasehagen, L.J. "Integrated approach for ^{13}C NMR shift prediction, spectral simulation, and library search." Anal. Chim. Acta 285, 223-235, 1994.

[5] Doll, K. M. and Erhan, S. Z. "Synthesis of carbonated fatty methyl esters using supercritical carbon dioxide." J. Agric. Food Chem. 53, 9608-9614, 2005.

[6] Kappe, C. O., Murphree, S.S., and Padwa, A. "Synthetic applications of furan Diels-Alder chemistry." Tetrahedron 53(42), 14179-14233, 1997.

[7] Knothe, G. "Dependence of biodiesel fuel properties on the structure of fatty acid alkyl esters." Fuel Process. Technol. 86, 1059-1070, 2005.

[8] La Scala, J. and Wool, R. P. "Effect of FA composition on epoxidation kinetics of TAG." J. Am. Oil Chem. Soc. 79, 373-378, 2002.

[9] Liu, Z.S., Doll, K. M., and Holser, R.A. "Boron trifluoride catalyzed ring-opening polymerization of epoxidized soybean oil in liquid carbon dioxide." Green Chem. 11, 1774-1780, 2009.

[10] Liu, Z.S. and Erhan, S.Z. "Ring-opening polymerization of epoxidized soybean oil." J. Am. Oil Chem. Soc. 87, 437-444, 2010.

[11] Meier, A.R.M., Metzger, J.O., and Schubert, U.S. "Plant oil renewable resources as green alternatives in polymer science." Chem. Soc. Rev. 36, 1788-1902, 2007.

[12] MestReNova (NMR software with Predict feature), Mestrelab Research, Santiago de Compostela, Spain, 2014.

[13] Petrovic, Z.S., Zlatanic, A., Lava, C.C. and Sinadinovic-Fiser, S. "Epoxidation of soybean oil in toluene with peroxy acetic and peroxy formic acids – Kinetics and side reactions." Eur. J. Lipid Sci. Technol. 104, 293-299, 2002.

[14] Sharma, V. and Kundu, P. P. "Addition polymers from natural oils - A review." Prog. Polym. Sci. 31, 983-1008, 2006.

[15] Srivastava, A. and Prasad, R. "Triglycerides-based diesel fuels." Renewable and Sustainable Energy Reviews 4(2), 111-133, 2000.

[16] Tayde, S., Patnaik, M., Bhagt, S.L., and Renge, V.C. "Epoxidation of vegetable oils: A review." International Journal of Advanced Engineering Technology 2(4), 491-501, 2011.

[17] Ramadhas, A.S., Jayaraj, S., and Muraleedharan, C. "Use of vegetable oils as I.C. engine fuels—A review." Renewable Energy 29, 727–742, 2004.

[18] Rosatella, A.A., Simeonov, S.P., Frade, R. F. M., and Afonso, C. A. M. "5-Hydroxymethylfurfural (HMF) as a building block platform: Biological properties, synthesis and synthetic applications." Green Chem. 13, 754-793, 2011.

[19] van Putten, R.-J., van der Waal, J.C., de Jong, E., Rasrendra, C.B., Heeres, H.J., and de Vries, J.G. "Hydroxymethylfurfural, a versatile platform chemical made from renewable resources." Chem. Rev. 113, 1499–1597, 2013.

Sustainable Decision Support System for Crop Cultivation

Ghadiyali Tejas[1], Lad Kalpesh[2]

[1]UCCC & SPBCBA& UACCAIT, Veer Narmad South Gujarat University, Gujarat, India

[2]SRIMCA, Uka Tarsadia University, Bardoli, Gujarat, India

[1]tejas_ghadiyali@rediffmail.com; [2]kalpesh.lad@utu.ac.in

Abstract

Agricultural production in a farm is a complex process, which requires much knowledge about farming and related agricultural information. The farmer communities have to make complicated decisions during a short time. This process includes the choice of decisions about agro-business strategy and technology, and suitable timely decision-making contributes to maximize farm revenue. Mathematics and Information Technology are providing the resources to cope up with such situations. Decision Support System (DSS) estimates the efficiency of possible decisions, reduces uncertainty, and selects the best possible decisions. The main objective of the proposed DSS is to analyze meteorological parameters such as Temperature, Humidity and Rainfall and agriculture product 'Last Year Supply' data of last five years in the district of Surat (Gujarat, India) and thereby to predict agriculture product market price that ultimately helps the farmer community to take decisions prior to Crop Cultivation.

Keywords

Agriculture Intelligence; DSS in Agriculture; DSS in Crop Cultivation; Agriculture Product Price Prediction

Introduction

India is an agriculture dependent country and the farmer community of India is the backbone of the country. In India, more than 60% of the agriculture sector depends on the natural resources like rain and sun light for survival [1]. Approximately one-fifth GDP of India is contributed from this agriculture sector [2] and 69% of the population depends upon the rural economy for their livelihood [3]. "Climate variability in recent past and signals of climate change over the Indian region cause concern in the agricultural sector and also make farming more challenging in the country" [6]. Under such anomalies of meteorological parameters, more scientific and accurate information is needed by the farmers in the country for proper farm management including risk management and to further develop their adaptive capacity with improved planning and better management decisions.

The ultimate aim of the farmer community is to make profit from the sustainable cultivated agricultural product. At the time of agriculture product cultivation, the farmer community should have an idea about the price they will get in the market in future. This study aims at decision support at the time of crop cultivation for the farmer community by predicting agricultural product future market price. The agricultural commodity market price depends on various parameters like market price history as well as meteorological variations and 'Demand and Supply' theory. As a result, the commodity market prices observe considerable fluctuations. The researchers have been developing Agriculture Intelligence and this study is a part of it. The main objective of this DSS is to analyze market agriculture product 'supply' and linked meteorological parameters such as Temperature, Humidity and Rainfall in the determination of agricultural product market price in the district of Surat (Gujarat, India). The researchers have carried out different experiments using various parameters and have decided to involve selected parameters such as Meteorological Parameters and 'Last Year Supply' [33].

'Cobweb Theorem' [4] of agricultural product price policy determination says that, 'current year's price determines the next year's supply and next year's supply determines that year's price'. In support of the 'Cobweb Theorem', several econometrics literatures [21, 22 and 23] show that particular agriculture product supply determines the entire price strategies of that product in the market for the next year. So considering such theorem, the researchers would like to apply a new feature as 'Last Year Supply' in the prediction of agricultural product price determination. There are several DSS provided by government and private agencies in the domain of agriculture

2327-7246/15/02 036-10 © 2015 DEStech Publications, Inc.
doi:10.12783/ijast.2015.0302.02

sector [6 and 7] for farm management. The main goal of this study is to present the analysis of linked agriculture supply data with meteorological data that helps agriculture stakeholders in predictive agriculture product price, and thereby, help the farmer community in their risk management and betterment of their ultimate goal of profit making. In this study, the researchers performed several experiments for different agriculture commodities and prepared relative visuals in the form of comparative chart and determined accuracy using the statistical measure 'Mean Average Percentage Error'.

Literature Survey

In support of the 'Cob-Web Theorem' [4], several econometrics literatures [5, 23, 24 and 25] show that particular agriculture product supply determines the entire price strategies of that product in the market for the next year. 'Demand and Supply' theory also determines the supply of the agriculture product in the market. Agriculture product demands depend on population factor of that geographical region. Therefore, in the short run, demand will not drastically change and that is why agricultural product price strategies depend on the supply of that product.

[8], aimed at two different systems for analysis 'Farming System' and 'Management System'. They discussed about their 'farm production model' with two case studies of one with broad-scale commercial agriculture in northeastern Australia and the other with resource poor smallholder farmers in Africa and tried to simulate the biophysical performance of farm production systems. [9], developed a DSS that discussed about farm level indicators of sustainable land management development. This study made use of the Framework for Evaluation of Sustainable Land Management (FESLM) to determine the environmental, economic and social sustainability of major farming systems in the Prairie Region of Western Canada. Local knowledge obtained from questionnaires and interviews was conducted for addressing gaps in information requirements for sustainability assessment. They conclude with the remark that 'Incorporation of local farmer knowledge is essential to address data and information gaps'. [10], developed a 'The Panting Date Calculator' which is a decision support system for agriculture that assists farmer and crop consultants for scheduling planting. This tool was utilized to schedule planting and project the growing season based on historical climate data, risk tolerance, and other factors. The Planting Date Guide matches the climatic parameters such as frost-free period, growing degree-days, and relative maturity days for a selected field.

[11], suggested an engineering approach on mathematical models of systems and processes, contributed new methods that support decision making at all levels from strategy and planning to tactics and real-time control in farm management. Their results indicate that, Precision in decision making leads to decreased use of inputs, less environmental emissions and enhanced profitability – all essential to sustainable agriculture systems. [12], have evaluated the significance of meteorological parameters in the implementation of agriculture engineering practices in the Tabuk region of the Royal Kingdom of Saudi Arabia. In this study, they observed that among all the meteorological parameters, temperature and relative humidity greatly influence the production of crops like wheat, potato, fruits and vegetables in this region. [13], have studied the importance of meteorological variables in the bias of Potential evapotranspiration estimated in Crete, Southern Greece. In this study, they have used Principal Component Method (PCM) as extraction method and then step wise Multiple Linear Regression Method (MLRM) was performed. Both factor and regression analyses were performed in Statistical terms (StatSoft-2007). The result was shown for the correlation coefficients between the daily meteorological observation and other factors.

All the above and other literature reviews related to DSS [14, 15 and 16] as well as meteorological parameter analyses [17,18,19 and 20] in this domain, directly or indirectly refer to the decision support in agriculture production and impact of meteorological parameters in various agriculture field operations such as sowing, water management, crop protection, soil management, and harvesting. Various price prediction and price forecasting approaches have been suggested by [24-30] in the domain of agricultural product price determination. In this study, the researchers intend to show the relevance of meteorological parameters linked with agriculture supply in the agriculture product market price determination. Trustworthy agriculture-product supply data and meteorological data also help to optimize planting schedules, growing days, irrigation needs, and harvest time. Reduced chemical, pesticide, and fertilizer spraying volumes are also an important outcome of in-time prior crop cultivation decision making.

Data Collection and Preprocessing

The researchers have collected the history price and supply data from the Agriculture web portal, www.agmarknet.nic.in of Government of India, from 1st January 2009 to 31st December 2014. Meteorological data like 'Humidity', 'Temperature' and 'Precipitation' (Rainfall) was collected from IMD (India Meteorological Department) for the base station 'Surat' for the same period.

Such collected meteorological data has been pre-processed and set in line with the daily average agriculture commodity market price data for the same date to perform further analysis. At the same time using some line of code, the researchers also set in line the 'Last Year Supply' data for the respective agriculture commodity for the same date. Here the data filled as the 'average supply of that week' for which the 'Last Year Supply' was not found and thus it ensured value for every day supply for existing data. The researchers have selected ten Agriculture Commodities such as 'Lady Finger (Bhindi)', 'Brinjal', 'Cabbage', 'Cauliflower', 'Green Chilly', 'Lemon', 'Onion', 'Potato', 'Surat Beans (Papadi)' and 'Tomato' for the entire said period of the analysis.

TABLE 1. EXPERIMENT DESIGN: AGRICULTURE COMMODITY-BHINDI (LADY FINGER)

Expr. Sr. No.	Data Used For Last Years	Parameter Used						Para. Pred.	Tool / Method Used	Mape
1	5	O_P	-	-	-	-	-	P_S	Wessa (L)	-
	4	O_P	-	-	-	-	-	P_S	Wessa (L)	-
	3	O_P	-	-	-	-	-	P_S	Wessa (L)	-
	2	O_P	-	-	-	-	-	P_S	Wessa (L)	-
	1	O_P	-	-	-	-	-	P_S	Wessa (L)	-
2	5	P_S	-	-	-	-	-	PRC	Wessa (L)	0.2384
	4	P_S	-	-	-	-	-	PRC	Wessa (L)	0.2404
	3	P_S	-	-	-	-	-	PRC	Wessa (L)	0.2379
	2	**P_S**	**-**	**-**	**-**	**-**	**-**	**PRC**	**Wessa (L)**	**0.2154**
	1	P_S	-	-	-	-	-	PRC	Wessa (L)	0.2211
3	5	P_S	-	-	-	-	-	PRC	Wessa(Q2)	0.2403
	4	P_S	-	-	-	-	-	PRC	Wessa(Q2)	0.2401
	3	P_S	-	-	-	-	-	PRC	Wessa(Q2)	0.2372
	2	**P_S**	**-**	**-**	**-**	**-**	**-**	**PRC**	**Wessa(Q2)**	**0.2155**
	1	P_S	-	-	-	-	-	PRC	Wessa(Q2)	0.2227
4	5	O_P	-	-	-	-	-	PRC	MATLAB nntool	0.2499
	4	O_P	-	-	-	-	-	PRC	MATLAB nntool	0.2400
	3	O_P	-	-	-	-	-	PRC	MATLAB nntool	0.2350
	2	O_P	-	-	-	-	-	PRC	MATLAB nntool	0.2559
	1	O_P	-	-	-	-	-	PRC	MATLAB nntool	0.3640
5	5	TM	HM	RF	SPL	-	-	PRC	MATLAB nntool	0.2190
6	5	TM	HM	RF	SPL	LYP	-	PRC	MATLAB nntool	0.2278
7	**5**	**TM**	**HM**	**RF**	**LYS**	**-**	**-**	**PRC**	**MATLAB nntool**	**0.1813**
8	5	TM	HM	RF	LYS	-	-	PRC	Wessa (L)	0.2027
9	5	TM	HM	RF	LYS	SPL	-	PRC	MATLAB nntool	0.2396
10	5	TM	HM	RF	LYS	LYP	-	PRC	MATLAB nntool	0.2490
11	5	TM	HM	RF	LYS	SPL	LYP	PRC	MATLAB nntool	0.2722

O_P-Old Price, SPL-Supply, P_S-Predicted Supply TM-Temperature, HM-Humidity, RF-Rain Fall, LYS-Last Year Supply, LYP – Last Year Price, PRC-Price

Experiment Design and Methodology

After the data was pre-processed, the researcher carried out eleven different experiments with sub-experiments using various meteorological parameters as well as other parameters such as 'Old Supply', 'Old Price' and 'Current Supply' to predict the future agriculture commodity price using last five years' data. As shown in [3], other than this, the researchers also applied various ranking algorithms to decide the meteorological parameters in further experiments. Through these experiments, the researchers decided to involve selected parameters Temperature, Humidity and Rainfall as Meteorological Parameters and 'Old Supply' that support 'Cob-Web Theorem', for further analysis. The experiment inputs, parameter and technology or tools used are as mentioned in table 1.

As shown in table 1, the researchers started experiments with Sr. No. 1 and 2 as per the 'Cob-Web Theorem', which says that 'current year's price determines the next year's supply and next year's supply determines that year's price'. So here, Sr. No. 1 indicates the prediction of next year's supply (Predicted Supply – P_S) using old year's price (O_P). Such predicted supply (P_S) was used for experiments Sr. No. 2 to predict Price (PRC) for all last 5 years' data. Here the researchers would like to note that, as per the 'Cob Web Theorem' only the last year data predicts the next year's price. However, these experiments show that the result will be better, if we consider last two years' supply data rather than considering only the last year supply data, for future price prediction. Further, the experiment design Sr. No. 7 shows that, meteorological parameters - Temperature (TM), Humidity (HM) and Rain Fall (RF) and Last Year Supply (LYS) as input data, predict future Price (PRC) with higher accuracy compared to the rest experiment designs. So the researchers selected these parameters for all further experiments with last five years' data i.e. from 1st January 2009 to 31st December 2013 as the training data and Last One year data i.e. from 1st January 2014 to 31st December 2014 as testing data. The researchers designed the experiments using the online statistical tool 'Wessa' (Web-enabled scientific services and applications) [34] with linear and non-linear regression analysis and 'nntool' of Matlab (R2012a) with 'feed forward back-propagation' algorithm. Experiment design results show that linear and non-linear regression has very less amount of variation in prediction of the future price.

Pre-processed data has applied to Multiple Regression Analysis methodology using Statistical tool (Wessa) and evaluated results of estimated regression equation in the form of multiple parameters of single equation have generated. In this equation Temperature, Humidity, Rainfall, Last Year Supply are independent variables and

Predicted Price is dependent variable as follows:

$$\textbf{Price } (\tilde{Y}) = ß_0 + ß_1 * X_1 + ß_2 * X_2 + ß_3 * X_3 + ß_4 * X_4$$

Where, $\hat{Y}$= Predicted Market Price

$X1$ = Temperature

X_2 = Humidity

X_3 = Rainfall and

X_4 = Last Year Supply

$ß_0$ = Intercept

n = number of observations

$ß_0 = \overline{Y} + ß_1 * \overline{X1} + ß_2 * \overline{X2} + ß_3 * \overline{X3} + ß_4 *$

$ß_i$, i = 1 to 4 can be calculated as follows:

$$ß_i = \frac{\sum(Xi * Y) - \frac{(\sum Xi)*(\sum Y)}{n}}{\sum(Xi^2) - \frac{(\sum Xi)^2}{n}}$$

Experiments have also been performed in the Artificial Neural Network using nntool of MATLAB. In this tool, Training data was given in the form of four Input Data and one Target Data. Testing data in this tool was treated as 'Sample Data'. On the basis of such applied data, the output data in the form of Predicted Price data was generated after applying training and having simulation on such sample data. At the time of creating and training the Artificial Neural Network using nntool of MATLAB, the 'Feed forward Back Propagation' algorithm has been used. This kind of neural network consists of three layers—the input layer, hidden layer(s), and output layer. These layers are connected to each other and the output of each previous layer becomes the input to the next layer. In this

experiment Inputs 'Temperature', 'Humidity', 'Rainfall' and 'Last Year Supply' are weighed and sent to processing neurons in the next layers. This Artificial Neural Network contains four input layers and one output layer that act like independent and dependent variables in a regression model. The number of neurons in the input and output layers relates to the number of parameters taken from the problem and equals to independent and dependent variables. The hidden layers play a very important role in the successful application of ANNs. The hidden neurons in the hidden layer allow ANNs to capture the pattern in the data and allow the network to generate numerous relationships between the inputs and outputs. One hidden layer may be enough for most forecasting problems. The hidden layer might contain one or more neurons, the single hidden layer feed forward network have calculated as follows:

$$\textbf{Price (Y) = G (} \ a_0 + \sum_{j=1}^{p} aj \quad \textbf{F (} b_{0j} + \sum_{j=1}^{q} bji * Xi \ \textbf{))}$$

where $\mathbf{Y}$ is the output layer with one neuron and $\mathbf{X}_i$ is the i th input. Any hidden layer unit receives the weighted sum of all inputs and a bias term ($\mathbf{b}_{0j}$) and produces an output signal through the hidden transfer function ($\mathbf{F}$). Where $\mathbf{b}_{ij}$ is the weight of its connection from the i th input unit to the j th hidden layer unit. Similarly, the output unit receives the weighted sum of the output signal of the hidden layer with a bias term ($\mathbf{a}_0$), and produces a signal through the output transfer function ($\mathbf{G}$). Where $\mathbf{a}_j$ is the weight of the connection from the j th hidden layer. Where p and q represent the number of neuron in hidden and input layers.

The researchers evaluated the results using measures for forecasting Mean Absolute Percentage Error (MAPE). The researchers have also shown the predicted trend of selected commodity in the form of graphical notation for visual convenience. In this study, the researchers have also tried to compare the outcomes of Statistical technique Multiple Regression Analysis with the outcomes of the data mining techniques Neural Networks, and accordingly have shown the results and analyses of the experiments.

$$MAPE = \frac{1}{n} * \sum_{i=1}^{n} \frac{Abs(Yi - \bar{Y})}{Yi} \quad \text{and} \quad \textbf{Accuracy \% = (1 – MAPE) * 100}$$

Experimental Result and Analysis

Analysis and result for the meteorological data has been done using the Statistical techniques (multiple regression analysis) and data mining techniques (Neural Network) during the different agricultural commodities for the period January 2009 to December 2013 and tested for the period January 2014 to December 2014. The researchers have prepared the following analysis table with estimated linear regression equation that helps us to analyze the accuracy of both the techniques. This table compares both the techniques using the forecasting measures Mean Absolute Percentage Error (MAPE). Comparative analysis is shown in Table 2.

TABLE 2. COMPARATIVE ANALYSES FOR AGRICULTURE PRODUCT PRICE PREDICTION WITH MRA BETA VALUE

SR	Agriculture Commodity	MAPE		Multiple Regression Analysis ' ßeta' Value				
		Neural Network MATLAB (nntool)	Multiple Regression Analysis (WESSA)	Intercept ß0	Temperature ß1	Humidity ß2	Rainfall ß3	Old Year Supply ß4
01	Bhindi	0.2163	0.2022	4431.25	-66.8477	-11.3193	1.3691	0.3660
02	Cualiflower	0.2840	0.2821	1773.98	-30.9477	5.1724	-2.7563	-1.4173
03	Greenchilly	0.3443	0.3377	-715.86	71.3193	4.6177	3.1988	13.4900
04	Onion	0.3442	0.2723	2852.80	-62.4558	6.3378	-2.7188	-2.1713
05	Potato	0.3921	0.4073	909.19	4.2734	2.3973	-0.0075	-0.8776
06	Surat Beans	0.2629	0.2329	-945.03	147.7161	15.1438	-2.8844	37.2132

In the agricultural commodity market, the price of the agricultural product depends on the 'Seasonal' factors. To enhance the accuracy level, the researchers have classified the entire year data into three seasonal compartments viz. 'Winter', 'Summer' and 'Monsoon'. Here in these experiments, 'Winter' season considers the data for the months of Nov, Dec, Jan and Feb. 'Summer' season considers the data for the months of Mar, Apr, May and Jun. And 'Monsoon' considers the data for the months of Jul, Aug, Sep and Oct. For visual convenience, the researchers have showed few agricultural products seasonal for analysis in graphical form as indicated in figs. 1 to 6. These figures explain the prediction accuracy by the product price for different seasons.

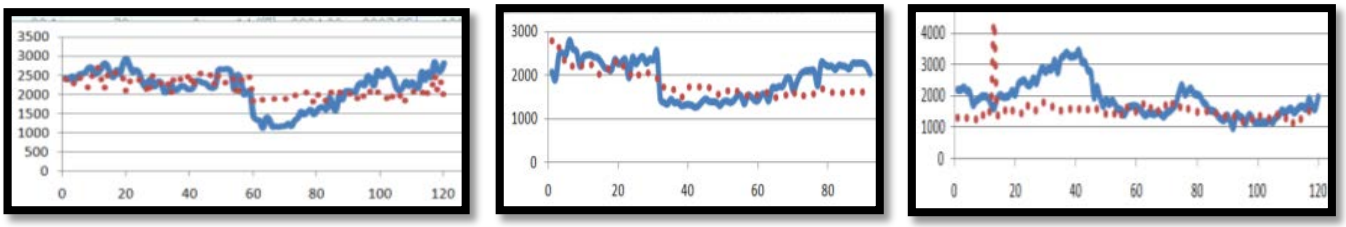

Winter Summer Monsoon

FIGURE 1. BHINDI (LADIES FINGERS)

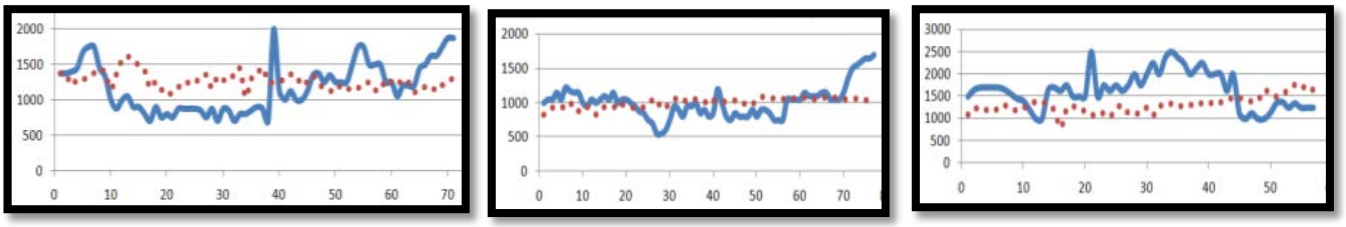

Winter Summer Monsoon

FIGURE 2. CAULIFLOWER

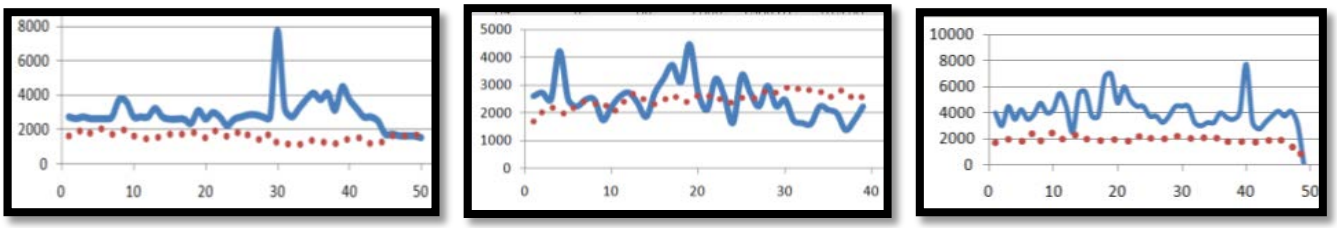

Winter Summer Monsoon

FIGURE 3. GREEN CHILLY

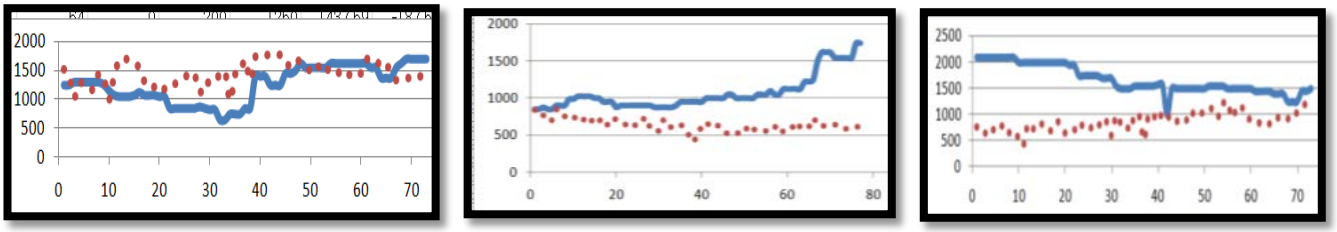

Winter Summer Monsoon

FIGURE 4. ONION

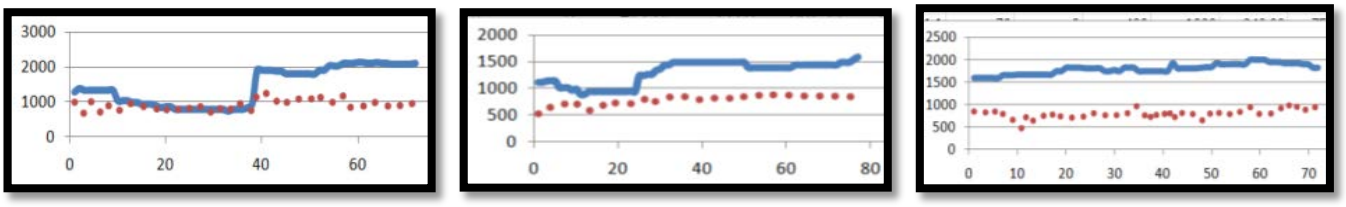

Winter Summer Monsoon

FIGURE 5. POTATO

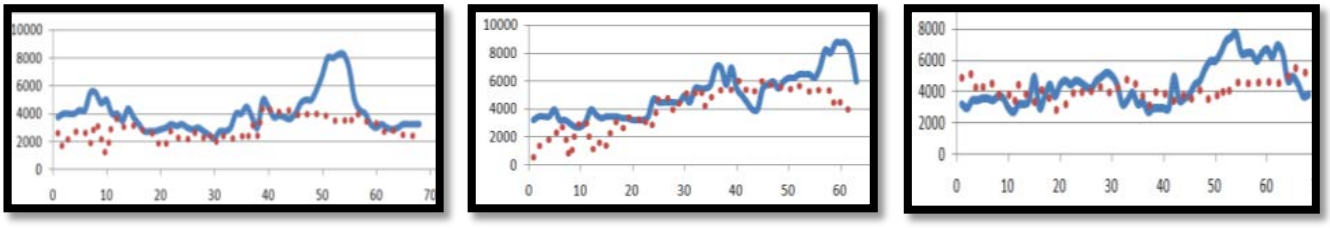

Winter Summer Monsoon

FIGURE 6. SURAT BEANS (PAPDI)

Considering the inflation rate in the agricultural product price, the researchers calculated the percentage change in price for particular agricultural commodity (Table 3) and calculated the average percentage change in price using the statistical techniques 'weighted moving average'. Applied modifications 'before' and 'after' considering percentage change in price are shown in figures 7 and 8.

TABLE 3. CALCULATED WEIGHTAGE MOVING AVERAGE PERCENTAGE CHANGE IN PRICE

SR	Agriculture Commodity	AVERAGE PRICE					Average % Δ in Price
		2009	2010	2011	2012	2013	
1	Bhindi (Lady Finger)	1309.71	1875.94	1744.39	2562.33	2440.68	
	(% Δ in Price)		43.23	-7.01	46.89	-4.75	19.59
2	Green Chilly	1393.00	1798.98	1762.17	2159.57	2948.01	
	(% Δ in Price)		29.14	-2.05	22.55	36.51	21.54
	Weightage per Year ➔		1.00	2.00	3.00	6.00	

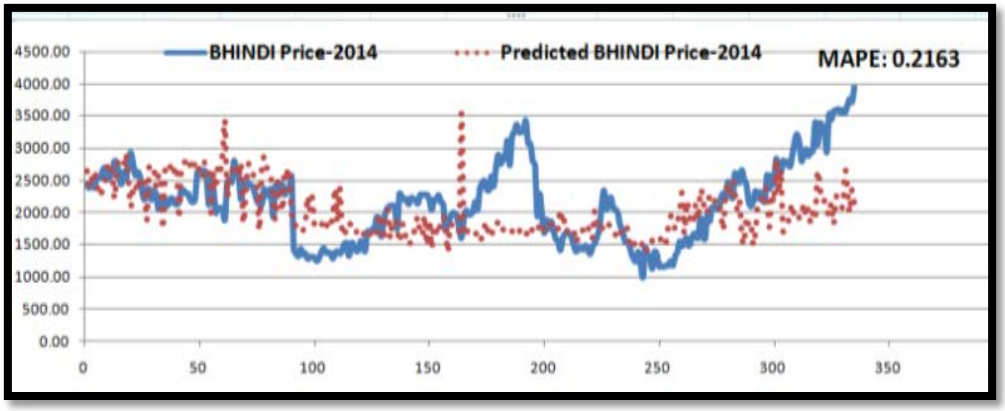

FIGURE 7. AGRICULTURE COMMODITY PREDICTED PRICE BEFORE CONSIDERING PERCENTAGE CHANGE IN PRICE

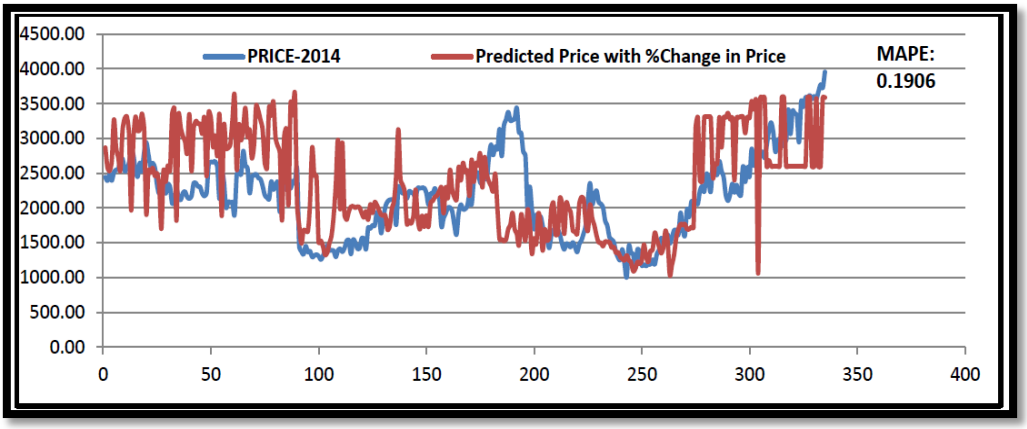

FIGURE 8. AGRICULTURE COMMODITY PREDICTED PRICE AFTER CONSIDERING PERCENTAGE CHANGE IN PRICE

The above tables and figures indicate the accuracy level is higher than that of the accuracy achieved earlier using 'only price history' data or using 'only meteorological data' without considering change in price. Therefore, the researchers infer that 'last year supply' data when properly linked with meteorological data, impacts reasonably on the future price prediction of agricultural product. In this study, the researchers have tried to enhance the accuracy of the predicted data in different scenarios such as 'Seasonal Prediction', 'Prediction with considering Percentage Change in price' (yearly) and even by converting the training data in the form of the 'Bi-variants Matrix' of 'Month-Day of Month v/s years'. Such decision support can also be useful to the body or group of persons who involve in formulation of 'Minimum Support Price'. Such DSS can be utilized for the betterment of 'Agriculture Intelligence'

in the better decision-making process of agriculture stakeholders. As the researchers have included last five years' data, the processing of data availability takes less time that gives the 'Sustainability' factor to such DSS. During the study, the researchers conducted many experiments and based on the results generated the researchers would like to infer that 'Last Year Supply data of the agriculture products is involved in future price determination of agriculture products'.

Conclusions

Based on the experiments conducted by the researcher in this study, the researcher would like to conclude that Last Year Supply affects significantly when it is properly linked with meteorological parameters that influence climate variability and thereby crop production quality and crop price. Agriculture commodity market is a highly fluctuating market and the price of the agricultural product depends on so many parameters other than those analyzed by the researchers have in this study. Still, the researchers have achieved more than 80% of accuracy in the selected agricultural commodities. Such predicted price data helps the farmer community and the agriculture consultants in their decision making for cultivation, scheduling planting, planning and other farm management tasks such as irrigation planning, purchase of pesticides etc. prior to crop cultivation. This DSS can also be useful to agriculture stakeholders other than farmers such as Agricultural Consultants, Agri-Business Brokers, Minimum Support Price Recommendation Agencies, APMC Brokers and many more. The potential benefit of these DSS lies in assisting the agricultural product producers in making better-informed decisions.

REFERENCES

[1] Golait 2007. "Current Issues in Agriculture Credit in India: An Assessment", Reserve Bank of India Occasional Papers, 28(1):1-2.

[2] Government of India Planning Commission 2007. "Report of the Working Group on Agriculture Research and Education for the Eleventh Five Year Plan", pp.16-17.

[3] Planning Commission, Government of India 2007. "Eleventh Five Year Plan 2007–12", Agriculture, Rural development, Industry, Service and physical infrastructure, Vol. III.

[4] M Mordecai Ezekiel (1938). 'The Cobweb Theorem', Quarterly Journal of Economics, J-STOR, Oxford University Press, 52(2):255-280.

[5] D Daniel Dufresne and Felisa Vázquez (2012). 'Cobweb Theorems with Production Lags and Price Forecasting", Economics E-journal, 17.

[6] C.W. Fraisse , N.E. Breuer , D. Zierden , J.G. Bellowc, J. Pazd, V.E. Cabrera et.al. (2006). "AgClimate: A climate forecast information system for agricultural risk management in the southeastern USA", 'Computer and Electronics in Agriculture" Science Direct, Elsevier, 53:13-27.

[7] Ayubu J. Churi, Malongo R. S. Mlozi, Henry Mahoo, Siza D. Tumbo, Respickius Casmir (2013). "A Decision Support System for Enhancing Crop Productivity of Smallholder Farmers in Semi-Arid Agriculture", International Journal of Information and Communication Technology Research, ISSN: 2223-4985, 3(8):238-248.

[8] Simone Graeff, Johanna Link, Jochen Binder and Wilhelm Claupein (2012). "Crop Model as Decision Support System in Crop Production", 'Crop Production Technology'- ISBN 978-953-307-787-1, 3-28.

[9] Ranya Elsheikh, Abdul Rashid B. Mohamed Shariff, Fazel Amiri, Noordin B. Ahmad, Siva Kumar Balasundaram and Mohd Amin Mohd Soon (2013). 'Agriculture Land Suitability Evaluator (ALSE): A decision and planning support tool for tropical and subtropical crop', 'Computer and Electronics in Agriculture', Elsevier 93 : 98-10.

[10] B. A. Keatinga and R.L. McCown (2001). 'Advances in farming systems and analysis and intervention', Agricultural System, 'Elsevier' publication. 70 : 555-579.

[11] S.Gameda, J. Dumanski and D. Acton (1999). 'Farm Level Indicators of Sustainable Land Management for the Development of Decision Support Systems', Research Branch Agriculture and Agri-Food Canada, 1-9.

[12] Stephen E. Reichenbach, William J. Waltman, Gautam Jindal, L.A. Nelson, S.J. Meyer, J.S. Peake5, W. Fithian, and P.

Dappen (2003). "The Planting Date Calculator: A Decision support Tool for Agriculture', Computer Science and Engineering Department, University of Nebraska – Lincoln.

[13] W Day*, E. Audsley† and A. R. Frost (2008).).'An engineering approach to modeling, decision support and control for sustainable systems' an online journal 'Philosophical Transaction of Royal Society', doi:10.1098/rstb.2007.2168, 363: 527–541.

[14] P rof Dr Lekshmi Vijayan and Dr Fatema Abdullah Al Talhi (2013). "Significance of Meteorological Parameters in the Implementation of Agriculture Engineering Practices in and Around Tabuk Region, KSA", International Journal of Applied Science and Technology, 3(5):53-65

[15] Fotios Xystrakis and Andreas Matzarakis (2008). "The importance of meteorological variables in the bias of Potential evapotranspiration estimates in Crete, southern Greece", pp:96-100.

[16] Sergei Soldatenko and Lev Karlin (2014). "The Climate Change Impact on Russia's Wind Energy Resource: Current Areas of Research", Energy and Power Engineering, Scientific Research Publishing, doi: dx.doi.org/10.4236/epe.2014.611032, 6:371-385.

[17] Li Xiaoli, Yingyi Chen And Li Daoliang (2009). "A Spatial Decision Support System for Land-use Structure Optimization", WSEAS Transaction on Computer, 3(8):439-448.

[18] Anurag Agrahari and Dr. ShashiKant Tripathi (2012). 'A Theoretical Framework for Development of Decision Support System for Agriculture', 'Reseach Inventy', An Internation journal of Engineering and Science. Oct-2012, ISSN: 2278-4721. 1(6): 50-55.

[19] M.Durban and C.A. Glasbeyy (2001). "Weather modeling using multivariate latent Gaussian Model", Journal of 'Agriculture and Forest Meteorology', 109: 187-201.

[20] P.Roudier, B. Muller, P. d'Aquino, C. Roncoli, M.A. Soumaré, L. Batté and B. Sultan (2014). "The role of climate forecasts in smallholder agriculture: Lessons from participatory research in two communities in Senegal", Climate Risk Management. 2 : 42–55.

[21] Holzkämper, P. Calanca and J. Fuhrer(2011)."Analysing climate effects on agriculture in time and space", 'Procedia Environmental Sciences'. Science Direct, Elsevier, 3:58–62.

[22] Chaurasia, R.; P.K. Sharma; G.S. Mahi and S. Gurmit Singh (1991). "Climatic change and wheat yield in semi-arid region of Punjab-India, Proceedings of 'Asian Conference on Remote Sensing', ACRS-199.

[23] Serena Brianzoni, Cristiana Mammana, Elisabetta Michetti and Francesco Zirilli (2008). "A Stochastic Cobweb Dynamical Model", 'Discrete Dynamics in Nature and Society', Hindawi Publishing Corporation, Article ID 219653, doi:10.1155/2008/219653, 1-16.

[24] Cars Hommes, Joep Sonnemans, Jan Tuinstra, and Henk Van De Velden (2007). "Learning in Cobweb Experiments", Macroeconomic Dynamics, DOI: 10.1017/S1365100512060208, 11(1): 8-33.

[25] Klaus Reiner Schenk–Hopp´ (2002). "Resuscitating the Cobweb Cycle", working paper series ISSN-1424-0459, 'Institute of empirical research in Economics', Paper No. 123, 1-5.

[26] Ticlavilca, A. M., Dillon M. Feuz and Mac McKee. 2010. "Forecasting Agricultural Commodity Prices Using Multivariate Bayesian Machine Learning Regression." Proceedings of the NCCC-134 Conference on Applied Commodity Price Analysis, Forecasting, and Market Risk Management. St.Louis, MO. [http://www.farmdoc.illinois.edu/nccc134]

[27] Octavio A. Ramirez and Mohamadou Fadiga 2003. "Forecasting Agricultural Commodity Price with Asymmetric-Error GARCH Models" Journal of Agricultural and Resource Economics 28(1):71-85.

[28] P. Geoffrey Allen,1994. "Economic forecasting in agriculture", International Journal of Forecasting, Elsevier publication, 10:81-135

[29] Somayeh Ebrahimi, Shahrokh Shajari, Mohammad Hassan Tarazkar 2012. "Prediction of Agricultural Commodity Price Using Artificial Neural Networks: Case of Chicken Price in Fars province, Iran", J. Basic. Appl. Sci. Res., 2(11)11537-11541.

[30] Terry L. Kastens, Ted C. Schroeder, and Ron Plain 1998. "Evaluation of Extension and USDA Price and Production Forecasts", Journal ofAgricultural and Resource Economics 23(1):244-261.

[31] Tareq F. Khan, S. M. Sayem and M. S. Jahan 2010. "Forecasting Price of Selected Agricultural Commodities in Bangladesh: An Empirical Study", ASA University Review, 4(1): 15-22.

[32] Reza Moghaddasi and Bita Rahimi Badr 2008. "An Econometric Model for Wheat Price Forecasting in Iran", Conference Proceedings of International Conference on Applied Economics-ICOAE2008 671-678.

[33] Tejas Ghadiyali and Kalpesh Lad (2015). "Role of Meteorological Parameters in Agriculture Intelligence", Conference Proceeding 'International Conference of Recent Trend in Information Technology', ISBN: 978-81-928189-5-5, 108-114.

[34] Wessa, P. (2015). Free Statistics Software, Office for Research Development and Education, version 1.1.23-r7, URL http://www.wessa.net

[35] www. agmarknet.ac.in visited on 28/01/2015 at 7.30 p.m.

[36] www. itcportal.com visited on 03/01/2015 at 09.15 a.m.

[37] www.agriwatch.com visited on 03/01/2015 at 11 a.m.

[38] www.imd.`/2015 at 10.15 a.m.

[39] www.imd.gov.in on 08/02/2015 at 10.15 a.m.

[40] www.kisan.com visited on 08/12/2014 at 5.30 p.m.

Mr. Tejaskumar R. Ghadiyali was born in Surat, Gujarat, India on 20th October 1972. He completed his Bachelors in Science (B.Sc.-Physics) degree from 'Navyug College' affiliated to Veer Narmad South Gujarat University, Surat, Gujarat in 1993. He completed his Post Graduate Diploma in Computer Application (PGDCA) from VNSGU, Surat, Gujarat in 1996 and Master of Computer Application (MCA) from Indira Gandhi National Open University, New Delhi, India in 2002. His major field of study is Computer Science.

He is serving as an ASSISTANT PROFESSOR in "Udhna Citizen Commerce College & SPB College of Business Administration & Udhna Academy College of Computer Application & IT", Surat, Gujarat, India, since July 2002. He has published more than 10 research articles in various national and international journals. His research interests are 'Data Mining' and 'Agriculture Informatics'.

Mr. Ghadiyali is a life time member of INSAIT (Indian Society of Agricultural Information Technology), Dharwad, India. He is also a member of CSI (Computer Society of India) Surat Chapter, Gujarat, India. He is serving as a Member of Board of Studies (Computer Science & Information Technology), VNSGU, Surat, Gujarat, India since 2009.

Dr. Kalpesh B. Lad was born in Billimora, Gujarat, India on 1st August 1978. He completed his Bachelors in Science (B.Sc.-Computer Science) degree from 'Valod College' affiliated to Veer Narmad South Gujarat University, Surat, Gujarat in 1999 and Master in Computer Application (MCA) from Veer Narmad South Gujarat University, Surat,Gujarat, India in 2002. He completed his Doctorate in 2002 in the domain of 'System Software'.

He is serving as an ASSISTANT PROFESSOR in "Srimad Rajchandra Institute of Management and Computer Application" (SRIMCA), Uka Tarsadiya University, Bardoli, Gujarat, India, since 2002. He has published more than 30 research articles in various national and international journals. His research interests are 'Business Intelligence' and 'System Software'.

Dr. Lad is a member of ISTE (Indian Society for Technical Education) Bardoli, Gujarat, India. He is also a member of CSI (Computer Society of India) Bardoli Chapter, Gujarat, India. He is serving as a Member of Board of Studies (Computer Science & Information Technology), UTU, Surat, Gujarat, India since 2002. He is also serving as an active member of 'Syllabus Design Committee' of Master Course, 'Examiner Appointment Committee' and other University related core-committee.

Instant Pressure Drop Evaluation during Saturated Steam Puffing of Carrots

Hongbo Song, Suixiang Ma, Cairu Lai, Xiaoqi Wu, Fengping An, Jinhua Tong

College of Food Science, Fujian Agriculture and Forestry University, Fuzhou, China

sghgbode@163.com

Abstract

Vapor instant release and superheated liquid flash evaporation in foods are the two main factors in steam-puffing. The condensed water produced by saturated steam is absorbed by the food material, thereby increasing moisture content. A model, which incorporated moisture content, radius, mechanical properties of un-puffed materials, properties of saturated steam, was generated. Spherical carrots (diameter: 10±1 mm) were used. The results revealed that the puffing power model can be used to predict the relationship between puffing ratio (R^2 >0.95) and moisture content (20–32%), and the relationship between puffing ratio (R^2 >0.99) and saturated steam temperature (390–430 K). Sufficient moisture content was the basis for producing superheated liquid for puffing; superheated steam at high temperatures was necessary for the formation of superheated liquid and high vapor pressure values in food materials.

Keywords

Modelling; Power; Puffing; Instant Pressure Drop; Saturated Steam; Carrot

Introduction

Steam-puffing of foods occurs in two stages. In the first stage, food materials are heated by steam. In the second stage, the pressure in the heating chamber is released, and the volume of the food material increases due to pressure differences and flash evaporation ((Rezzoug et al., 2000; Mounir et al., 2011; Louka et al., 2004).

Foods consist of solids, moisture, and gas. Water in porous materials evaporates rapidly, leading to volume expansion (Datta 2007). Studies focused on far-infrared, heated air and high-power microwave-puffing revealed that moisture flash evaporation is crucial in puffing. Additionally, the puffing capacity of high-power microwave is greater than that of far-infrared, heated air (Nath et al., 2007; Rakesh et al., 2011). The relationship between food deformation and energy during bread baking reveals that the former is related to pressure gradient and that the pressure of internal water evaporation is greater than that of steam pressure (Zhang et al., 2005).

Solid mechanics allows the study of the relationship between mechanical properties and dynamics. Niamnuy et al. (2008) reported that volume changes of shrimp during spouted bed-drying were dependent on the mechanical properties and the gas in food material. The mechanical behavior of microwave vacuum-dried dough has been described using a finite element method (Ressing et al., 2007). The duration of material expansion and deformation in these studies was significant; therefore, these studies may not be applicable in the steam-puffing of fruits and vegetables. The instant release of energy from superheated liquid is commonly reported in the food industry. When liquid achieves high temperatures, the liquid is referred to as a superheated liquid that has explosion capacity. At certain conditions, the liquid explodes, i.e., it becomes a "boiling liquid expanding vapor explosion" (Reid, 1979). Compressed liquefied gas involves gas and liquid phases; its energy is related to the volumes of gas and liquid (Gong et al., 2004; Lin et al., 2010; Prugh, 1991). Chen et al. (2008) reported that a two-phase layer forms on the liquid surface after the vessel is opened (3–4 ms), the whole liquid boils after about 17 ms, and the boiling of superheated liquid disappears from38 ms to 168 ms. Therefore, the energy release of superheated liquid occurs during a very short period of time.

The power of instant pressure drop in steam-puffing mainly includes two parts: internal gas pressure of the material and overheating degree of moisture. Quantitative studies on steam-puffing power have not been performed. Because there is a unique relationship between temperature and pressure in saturated steam, it is important to understand the steam-puffing mechanism. In this study, we discussed the role of gas and superheated

2327-7246/15/02 046-12 © 2015 DEStech Publications, Inc.
doi:10.12783/ijast.2015.0302.03

liquid in materials during saturated steam instant pressure drop.

Materials and Methods

Experimental Set-Up

A schematic diagram of a saturated steam puffing instrument (VP-100, Lizhong, Quanzhou, China) is shown in Fig. 1.

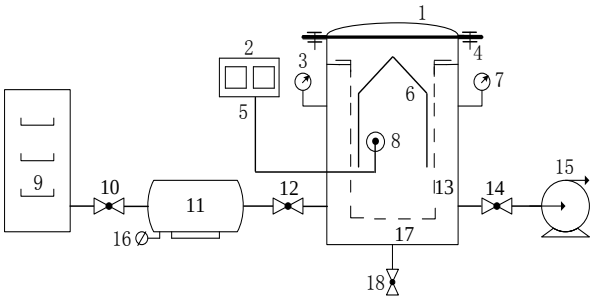

FIG. 1 SCHEMATIC DIAGRAM OF INSTANT PRESSURE DROP PUFFING WITH SATURATED STEAM.

(1)cover; (2) monitor; (3) thermometer; (4) locking bolt; (5) temperature sensor; (6) drain cover; (7) pressure gauge; (8) samples; (9) steam generator; (10) connection valve; (11) steam reservoir; (12) steam inlet; (13) sample holder; (14) vacuum valve; (15) vacuum pump; (16) steam trap; (17) puffing chamber; (18) decompression valve.

Steam, formed in the steam generator (9), is stored in the steam reservoir (11) through the connection valve (10). The steam inlet (12) and decompression valve (18) remain closed. A temperature sensor (5) is inserted in the sample core (8) and materials are loaded in the sample holder (13). After the cover (1) is closed and the locking bolt (4) is locked, the vacuum valve (14) is opened and the vacuum pump (15) is turned on. Gases in the puffing chamber and in the material are gradually removed. The vacuum valve (14) and vacuum pump (15) are closed, the steam inlet (12) is opened, and steam is transferred to the puffing chamber (17). When thermometer (3) and pressure gauge (7) reach desired values, the inlet valve (12) is adjusted to maintain a stable temperature and pressure. The core sample temperature, which is recorded by a temperature sensor (5), is continuously shown on a monitor (2). After a certain period of thermal treatment, the decompression valve (18) is opened instantly to allow sample puffing.

Sample Preparation

Fresh carrots (moisture content: 88.4%) were obtained from a local supermarket in Yonghui (Fuzhou, China). The carrots were stored at 3±1°C and 90–95% relative humidity for 14 d. Carrots (1 kg) of 50–55 mm diameter and 200–250 mm length were selected.

The carrots were washed, peeled, cut into spheres (diameter: 15 mm), and partially dehydrated in a hot-air dryer (PHG-9123A, Jinghong, Shanghai, China) at 70°C with an air velocity of 1.5 m/s. At final moisture contents of 20, 24, 28, and 32%, the carrots had a diameter of 10±1 mm. The samples were stored inside aluminum foil bags at 23±2°C for >2 h (Huang et al., 2012).

Core Temperature

The core temperature of the carrots was detected by a HH11B digital thermometer and a TT-K-30-SLE-1000 (2×φ 0.254 mm) thermoelectric couple (OMEGA instrument Co., Ltd, US). Fifteen pre-dehydrated carrot spheres were placed in the sample holder with a temperature sensor.

Moisture Content

The samples were dried to constant weight at 70°C and 133 Pa in a vacuum oven (DZF6050, Jinghong, Shanghai, China). Sample mass was measured on a balance (BSA124S, Sartorius LTD., Bejiing, China) before and after dehydration. Moisture content was calculated from mass difference and expressed as percentage of sample mass (Shyu et al., 2001; Acevedo et al., 2008).

Mass of Condensed Water

The mass of condensed water is the average absorbing water mass per sample. The mass of condensed water was calculated from the difference between the mass of pre-dehydrated carrot spheres and the mass of the sample relative to the number of samples.

Pore Volume

Pore volume is the difference between the apparent volume and the particle volume. The apparent volume was measured by immersing one sample in n-heptane (Krokida et al., 1999; Yan et al., 2008). Particle volume was measured with a gas pycnometer (G-DenPyc 2900, Beijing, China) using N_2 (Mayor et al., 2011; Sereno et al., 2007).

Young's Modulus

After the carrots were dried to a certain moisture content, the samples were cut into cylinders (10 cm in diameter × 10 cm in length) and placed on two parallel plates on a universal testing machine (59444, Instron (Shanghai) LTD., China) with a loading velocity of 20 mm/min (Nielsen et al., 1998). Young's modulus is the gradient of the initial linear slope of the loading curve (Cen et al., 2013). Sample diameter was recorded with a digital caliper (A635066, Ester Electrical Ltd., Shanghai, China). Poisson's ratio was calculated by Eq. (1) (Burubai et al., 2008):

$$v = \frac{\left(\frac{D_1 - D_0}{2}\right) \Big/ D_0}{(L_0 - L_1)/L_0} \tag{1}$$

where v is Poisson's ratio (non-dimensional), D_0 is the original sample diameter (mm), D_1 is the sample diameter after deflection (mm), L_0 is the original sample length (mm), and L_1 is the sample length after deflection (mm).

Puffing Ratio

Puffing ratio was used to compare the relative changes in sample volume before and after puffing. Puffing ratio was calculated by Eq. (2):

$$S = V / V_0 \tag{2}$$

where S is the puffing ratio (non-dimensional), V_0 is the sample volume before puffing (m^3), and V is the sample volume after puffing (m^3).

Modelling of Puffing Power

Pre-dehydrated material consists of solids, moisture, and gas. The gas is removed by vacuum prior to steam heating. Saturated steam enters the sample pores by pressure difference until the internal pressure is in equilibrium with the saturated steam pressure in the puffing chamber. During this process, there is heat exchange between the material and the saturated steam, resulting in the formation of condensed water. The water absorbed by the material decreases the material pores. When the decompression valve is opened, part of the superheated liquid and saturated steam in the material evaporates rapidly, resulting in material expansion. Therefore, puffing power is dependent on superheated liquid flash evaporation and saturated steam instant release.

Work of Saturated Steam

The saturated steam presented in the food material is considered to be an ideal gas. The work performed by the saturated steam during puffing can be calculated by Eq. (3) (Dang et al., 2010; Planas-Cuchi et al., 2011):

$$W_g = \frac{P_1 V_g}{k - 1}\left[1 - \left(\frac{P_2}{P_1}\right)^{\frac{k-1}{k}}\right] \tag{3}$$

where W_g is the work performed by the saturated steam (J), P_1 is the absolute pressure in the material before puffing (Pa), P_2 is the absolute pressure in the material after puffing (Pa), V_g is the vapor volume in the material before puffing (m^3), and k is the adiabatic exponent of saturated steam (non-dimensional).

For this study, material pores were filled with saturated steam after heating because the material gas was removed by vacuum before heating. Therefore, the vapor volume in the material was equivalent to the pore volume (Eq. 4):

$$V_g = V' \tag{4}$$

where V' is the pore volume in the material before puffing (m3).

Eq. (4) was substituted into Eq. (3), resulting in Eq. (5):

$$W_g = \frac{P_1 V'}{k-1}\left[1-\left(\frac{P_2}{P_1}\right)^{\frac{k-1}{k}}\right] \tag{5}$$

Work of Superheated Liquid

The work of superheated liquid was calculated by Eq. (6) (Wang et al., 2011),

$$W_l = \left[(h_1 - h_2) - (s_1 - s_2)T\right] m_l \tag{6}$$

where W_l is the work of the superheated liquid (J), h_1 is the specific enthalpy of liquid before puffing (J/kg), h_2 is the specific enthalpy of liquid after puffing (J/kg), s_1 is the specific entropy of liquid before puffing (J/[kg×K]), s_2 is the specific entropy of liquid after puffing (J/[kg×K]), T is the liquid boiling point under environmental pressure after puffing (K), and m_l is the liquid mass of flash evaporation (kg).

Excess heat caused by $h_1 > h_2$ supplies vaporizing energy to the superheated liquid. The material temperature decreases to the boiling temperature corresponding to the environmental pressure after puffing. According to the law of energy conservation, the heat balance equation is

$$h_1 = (1-x)h_2 + x\left(h_2 + h'\right) \tag{7}$$

$$x = \frac{h_1 - h_2}{h'} \tag{8}$$

where x is the flashing ratio (non-dimensional) and h' is the latent heat of vaporization under environmental temperature after puffing (J/kg).

The total water mass of the material can be calculated by Eq. (9),

$$m_w = m_0 \cdot w_0 + M \tag{9}$$

where m_w is the total water mass of the material before puffing (kg), m_0 is the mass of the pre-dehydrated material (kg), w_0 is the moisture content of the pre-dehydrated material (%), and M is the mass of condensed water (kg).

Taking into account Eq. (6), Eq. (8), and Eq. (9), the work equation of the superheated liquid was

$$W_l = \left[(h_1 - h_2) - (s_1 - s_2)T\right](m_0 \cdot w_0 + M)\frac{h_1 - h_2}{h'} \tag{10}$$

Puffing Power Equation

During the saturated steam-puffing process, tension-compression stress results in material volume expansion. Based on the relationship among stress, strain, and displacement, the elastic principle was implemented to establish a relationship between puffing ratio and puffing power.

Basic Equations of Elasticity in the Form of Spherical Coordinate

A three-dimensional spherical coordinate is shown as Fig. 2. At M (r,θ, ϕ), r is the distance between O and M, θ is the angle between the directed line segment and the positive z-axis, and ϕ is the angle between the semi-planes XOZ and MOZ.

The relationship between the rectangular and the spherical coordinates can be described by

$$x = r\sin\theta\cos\varphi,\ y = r\sin\theta\sin\varphi,\ z = r\cos\theta \tag{11}$$

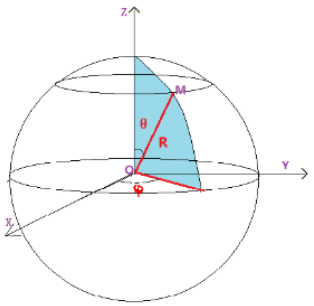

FIG. 2 REPRESENTATION OF MATERIAL IN SPHERICAL COORDINATE

The following assumptions were used to solve the problem:

(1)The material was continuous; its internal stress, strain, and displacement can be expressed as continuous functions.

(2)The material was homogeneous and isotropic.

(3)Material deformation was insignificant prior to puffing, and the displacement of every point was considerably less than the initial size of the material.

Stress, strain, and displacement of material were expressed by Eq. 12 (equilibrium differential equation), Eq. 13 (geometric equation), and Eq. 14 (constitutive equation) (Xue, 2006):

$$\begin{cases} \dfrac{\partial \sigma_r}{\partial r}+\dfrac{1}{r}\dfrac{\partial \tau_{\theta r}}{\partial \theta}+\dfrac{1}{r\sin\theta}\dfrac{\partial \tau_{\varphi r}}{\partial \varphi}+\dfrac{1}{r}(2\sigma_r-\sigma_\theta-\sigma_\varphi+\tau_{r\theta}\cot\theta)+F_{br}=0 \\ \dfrac{\partial \tau_{r\theta}}{\partial r}+\dfrac{1}{r}\dfrac{\partial \sigma_\theta}{\partial \theta}+\dfrac{1}{r\sin\theta}\dfrac{\partial \tau_{\varphi\theta}}{\partial \varphi}+\dfrac{1}{r}\left[(\sigma_\theta-\sigma_\varphi)\cot\theta+3\tau_{r\theta}\right]+F_{b\theta}=0 \\ \dfrac{\partial \tau_{r\varphi}}{\partial r}+\dfrac{1}{r}\dfrac{\partial \tau_{\theta\varphi}}{\partial \theta}+\dfrac{1}{r\sin\theta}\dfrac{\partial \sigma_\varphi}{\partial \varphi}+\dfrac{1}{r}\left[3\tau_{r\varphi}+2\tau_{\theta\varphi}\cot\theta\right]+F_{b\varphi}=0 \end{cases} \tag{12}$$

$$\begin{cases} \varepsilon_r=\dfrac{\partial u_r}{\partial r} \\ \varepsilon_\theta=\dfrac{u_r}{r}+\dfrac{1}{r}\dfrac{\partial u_\theta}{\partial \theta} \\ \varepsilon_\varphi=\dfrac{1}{r\sin\theta}\dfrac{\partial u_\varphi}{\partial \varphi}+\dfrac{u_\theta}{r}\cot\theta+\dfrac{u_r}{r} \\ \gamma_{r\theta}=\dfrac{1}{r}\dfrac{\partial u_r}{\partial \theta}+\dfrac{\partial u_\theta}{\partial r}-\dfrac{u_\theta}{r} \\ \gamma_{r\varphi}=\dfrac{1}{r\sin\theta}\dfrac{\partial u_r}{\partial \varphi}+\dfrac{\partial u_\varphi}{\partial r}-\dfrac{u_\varphi}{r} \\ \gamma_{\theta\varphi}=\dfrac{1}{r}(\dfrac{\partial u_\varphi}{\partial \theta}-u_\varphi\cot\theta)+\dfrac{1}{r\sin\theta}\dfrac{\partial u_\theta}{\partial \varphi} \end{cases} \tag{13}$$

$$\begin{cases} \sigma_\theta=\dfrac{E}{1+v}(\dfrac{v}{1-2v}\Theta+\varepsilon_\theta) \\ \sigma_r=\dfrac{E}{1+v}(\dfrac{v}{1-2v}\Theta+\varepsilon_r) \\ \sigma_\varphi=\dfrac{E}{1+v}(\dfrac{v}{1\text{-}2v}\Theta+\varepsilon_\varphi) \\ \tau_{\theta\varphi}=\dfrac{E}{2(1+v)}\gamma_{\theta\varphi} \\ \tau_{r\varphi}=\dfrac{E}{2(1+v)}\gamma_{r\varphi} \\ \tau_{r\theta}=\dfrac{E}{2(1+v)}\gamma_{r\theta} \\ \Theta=\varepsilon_r+\varepsilon_\theta+\varepsilon_\varphi \end{cases} \tag{14}$$

where u_r, u_θ, u_φ represent the displacement component (m) of the radial direction, colatitudes, warp direction, respectively, in the spherical coordinate; $\sigma_r, \sigma_\theta, \sigma_\varphi, \tau_{r\theta}, \tau_{\theta\varphi}, \tau_{r\varphi}$ are stress components (Pa); $\varepsilon_r, \varepsilon_\theta, \varepsilon_\varphi, \gamma_{r\theta}, \gamma_{\theta\varphi}, \gamma_{r\varphi}$ are strain force components (non-dimensional); E is the Young's modulus (Pa); v is Poisson's ratio (non-dimensional); and F is the external force (N/m^3).

Relationship between Puffing Power and Puffing Ratio

As a result of the spherical symmetric form, constraint conditions, external force, and other external factors were symmetric on one point. Due to symmetrical deformation, the problem could be simplified to $u_r = u_r(r)$, $u_\theta = u_\varphi = 0$. Based on geometric equation and constitutive equation, $\tau_{r\varphi} = \tau_{r\theta} = \tau_{\theta\varphi} = 0$ and $\gamma_{r\theta} = \gamma_{r\varphi} = \gamma_{\theta\varphi} = 0$. Based on the assumption of uniform puffing, deformation had only a radial direction; therefore, $\varepsilon_\theta = \varepsilon_\varphi = 0$, $\sigma_\theta = \sigma_\varphi = 0$. Consequently, Eq. (12), Eq. (13), and Eq. (14) were simplified to

$$\frac{\partial \sigma_r}{\partial r} + \frac{2\sigma_r}{r} + F_r = 0 \tag{15}$$

where F_r is the external force on a point, $F_r = F/V$ (N/m^3);

$$\varepsilon_r = \frac{\partial u_r}{\partial r} \tag{16}$$

$$\sigma_r = \frac{E}{1+v} \cdot \frac{1-v}{1-2v} \cdot \varepsilon_r \tag{17}$$

where $K = \frac{E}{1+v} \cdot \frac{1-v}{1-2v}$ (Pa)

Eq. (15) and Eq. (16) were expressed as

$$\frac{\partial^2 u_r}{\partial r^2} + \frac{2K}{r} \cdot \frac{\partial u_r}{\partial r} + F_r = 0 \tag{18}$$

Puffing deformation can have a radial variation, e.g., radius change:

$$u_r = \Delta r = r - r_0 \tag{19}$$

where r is the radius of puffed material (m) and r_0 is the radius of the material before puffing(m).

Eq. (19) was substituted into Eq. (18). F_r could be expressed as

$$F_r = -\frac{2K}{r} \tag{20}$$

The work W (J) done by F_r was expressed as

$$W = \frac{4}{3}\pi r_0^3 \int_{r_0}^{r} F_r \cdot dr \tag{21}$$

Eq. (21) was substituted into Eq. (20):

$$W = \frac{4}{3}\pi r_0^3 \cdot 2K(\ln r - \ln r_0) \tag{22}$$

Transforming Eq. (22) resulted in Eq. (23):

$$\frac{r}{r_0} = \exp\left(\frac{3W}{8K\pi r_0^3}\right) \tag{23}$$

Based on the definition, puffing ratio was expressed as Eq. (24):

$$S = \frac{V}{V_0} = \frac{\frac{4}{3}\pi r^3}{\frac{4}{3}\pi r_0^3} = \frac{r^3}{r_0^3} \tag{24}$$

Eq. (23) was substituted into Eq. (24), resulting in Eq. (25):

$$S = \exp\left(\frac{9W}{8K\pi r_0^{3}}\right) \tag{25}$$

Puffing energy was derived from two parts, saturated steam and superheated liquid. Total work was calculated by Eq. (26):

$$W = W_g + W_l \tag{26}$$

Eq. (26) was substituted into Eq. (25), obtaining the mathematical relationship between puffing power and puffing ratio:

$$\begin{aligned} S &= \exp\left[\frac{9(W_g + W_l)}{8K\pi r_0^{3}}\right] \\ &= \exp\left\{\frac{9}{8K\pi r_0^{3}}\left[\frac{P_1 V'}{k-1}\left(1-(P_2/P_1)^{\frac{k-1}{k}}\right)-\left[(h_1-h_2)-(s_1-s_2)T\right](m_0\cdot w_0+M)\frac{h_1-h_2}{h'}\right]\right\} \end{aligned} \tag{27}$$

Results and Analyses

The mass changes of pre-dehydrated spherical carrots (m_0) with different moisture contents are shown in Table 1.

TABLE 1 MASS OF SPHERICALLY-SHAPED CARROTS WITH DIFFERENT MOISTURE CONTENTS

w_0 (%)	m_0 (kg)
20	2.524×10^{-4}
24	2.649×10^{-4}
28	2.817×10^{-4}
32	3.011×10^{-4}

Physical Parameters

Condensed water was generated during the process of steam-heating, which condensed material moisture. Our experiments revealed that the core temperature of the carrots was very close to the temperature of saturated steam after 40 s of steam-heating. The mass of condensed water reached a maximum level; the moisture content of the carrots plateaued. Therefore, the physical parameters, such as pore volume, Young's modulus, and Poisson's ratio, were determined at a heating time of 40 s.

The condensed water mass of a single carrot sample (M) at 40 s heating time was measured (Table 2). Condensed water mass increased with increasing moisture content and saturated steam temperature.

Table 3 shows that material pore volumes decreased with increasing carrot moisture content and saturated steam temperature. There was more moisture in samples that had more condensed water produced by higher temperature heating (Table 2). Moisture occupied internal spaces with reduced pore volume.

Table 4 illustrates that Young's modulus slightly decreased with increasing moisture content and saturated steam temperature. A similar trend has been reported in carrots (Nielsen et al., 1998) and African Nutmeg (Burubai et al., 2007, 2008).

The results of Table 5 revealed that Poisson's ratio increased with increasing moisture content. At each moisture content, Poisson's ratio slightly increased while saturated steam temperature significantly increased due to more condensed water being produced during the heating period. Poisson's ratio varies between 0.23 and 0.49 for different materials (Burubai et al.,2007; Burubai et al.,2008). Golacki et al. (1998) and Maghsoudi et al. (2012) reported that the Poisson's ratio of carrots is 0.39–0.45, which was similar to the results obtained in this study. The variation trend of Poisson's ratio was different to that of moisture content. With increasing moisture content, Poisson's ratio decreased in African nutmeg (Burubai et al., 2008) and red bean grains (Mostafa et al., 2011) and increased in pistachios (Maghsoudi et al., 2012).

TABLE 2 CONDENSED WATER MASS IN CARROTS OF DIFFERENT MOISTURE CONTENTS BASED ON SATURATED STEAM TEMPERATURE

w_0 (%)	M (kg)				
	390 K	400 K	410 K	420 K	430 K
20	1.58×10^{-5}	1.70×10^{-5}	1.87×10^{-5}	2.10×10^{-5}	2.26×10^{-5}
24	1.80×10^{-5}	2.03×10^{-5}	2.21×10^{-5}	2.42×10^{-5}	2.57×10^{-5}
28	2.12×10^{-5}	2.35×10^{-5}	2.58×10^{-5}	2.80×10^{-5}	3.03×10^{-5}
32	2.42×10^{-5}	2.68×10^{-5}	2.97×10^{-5}	3.22×10^{-5}	3.48×10^{-5}

TABLE 3 PORE VOLUMES OF CARROTS OF DIFFERENT MOISTURE CONTENTS BASED ON SATURATED STEAM TEMPERATURE

w_0 (%)	V' (m^3)				
	390K	400K	410K	420K	430K
20	2.556×10^{-7}	2.539×10^{-7}	2.522×10^{-7}	2.505×10^{-7}	2.488×10^{-7}
24	2.406×10^{-7}	2.387×10^{-7}	2.367×10^{-7}	2.347×10^{-7}	2.327×10^{-7}
28	2.209×10^{-7}	2.186×10^{-7}	2.163×10^{-7}	2.140×10^{-7}	2.117×10^{-7}
32	1.982×10^{-7}	1.956×10^{-7}	1.929×10^{-7}	1.903×10^{-7}	1.876×10^{-7}

TABLE 4 YOUNG'S MODULUS OF CARROTS OF DIFFERENT MOISTURE CONTENTS BASED ON SATURATED STEAM TEMPERATURE

w_0 (%)	E (MPa)				
	390K	400K	410K	420K	430K
20	3.02	3.01	3.01	2.99	2.98
24	2.95	2.93	2.93	2.92	2.91
28	2.90	2.89	2.88	2.88	2.88
32	2.85	2.85	2.83	2.82	2.82

TABLE 5 POISSON'S RATIO OF CARROTS OF DIFFERENT MOISTURE CONTENTS BASED ON SATURATED STEAM TEMPERATURE

w_0 (%)	V				
	390K	400K	410K	420K	430K
20	0.34	0.34	0.34	0.35	0.36
24	0.37	0.37	0.37	0.38	0.38
28	0.39	0.39	0.39	0.40	0.40
32	0.40	0.40	0.41	0.42	0.42

TABLE 6 CHARACTERISTIC PARAMETERS OF SATURATED STEAM AT DIFFERENT TEMPERATURES

T_{sat} (K)	P_1 (Pa)	h_1 (J/kg)	s_1 (J/kg·K)
390	1.8×10^5	4.908×10^5	1.495×10^3
400	2.5×10^5	5.355×10^5	1.608×10^3
410	3.3×10^5	5.753×10^5	1.706×10^3
420	4.4×10^5	6.197×10^5	1.812×10^3
430	5.8×10^5	6.646×10^5	1.917×10^3

Parameters of Saturated Steam and Water

In this study, the temperature of saturated steam was 390–430 K; environmental pressure after puffing was standard atmospheric pressure. Saturated steam at different temperatures has different pressure values. The characteristic parameters of saturated steam at different temperatures (pressure) are shown in Table 6; the adiabatic index k of saturated steam is 1.135 (Yan et al., 2006). The pressure inside the material after puffing was standard atmospheric pressure, i.e., T= 373K, P_2= 1.0×105 (Pa), h_2= 4.175×105 (J/kg), s_2= 1.303×103 (J/kg·K), and h' = 2.258×105 (J/kg).

Effect of Moisture Content on Puffing Ratio

Carrots of different moisture contents were heated and puffed by saturated steam at 390, 400, 410, 420, and 430 K. The predicted puffing ratios were calculated by Eq. (27) and compared with the experimental values (Figures 3A–3E).

The predicted puffing ratio values were very close to the experimental values (R^2 >0.95). Puffing ratio increased with increasing moisture content from 20 to 32%. Higher moisture contents filled part of the pore material that decreased pore volume; therefore, the work performed by the vapor in the sample decreased. On the other hand, superheated liquid in the sample contributed to more moisture for flash evaporation, which produced strong

puffing power. Therefore, superheated liquid flash evaporation was more significant than vapor.

Our previous studies have shown that puffing ratio initially increases with increasing carrot moisture content up to 27% (Song et al., 2010). This result was probably attributed to that fact that as specific heat increases with increasing moisture content (Shmalko et al., 1996), more heat supplies energy for the high moisture material temperature to rise. Condensed water droplets produced by the heat exchange between the puffing chamber and steam were absorbed into the pores of the material, which partly filled pores and decreased the channels for puffing. In this study, the steam-puffing instrument was modified by adding a drain cover to the puffing chamber, which prevented the negative effects of the concentrated water droplets. As a result, the condensed water droplets were immediately removed to avoid unsufficient puffing.

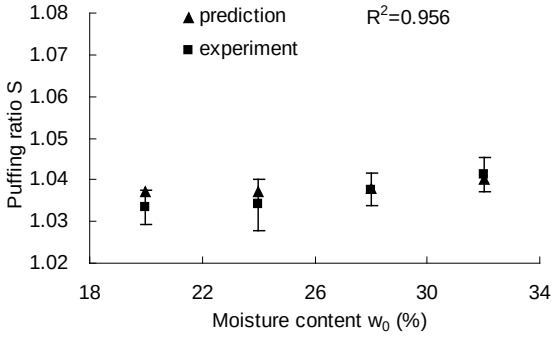

Fig. 3A (T_{sat}= 390 K)

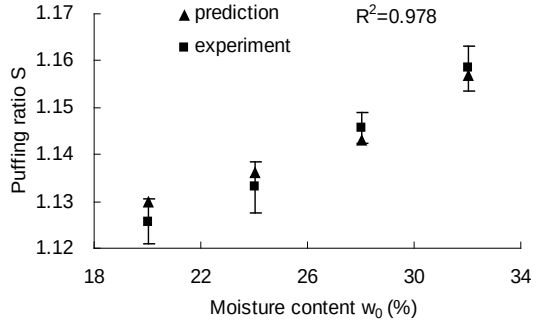

Fig. 3B (T_{sat}= 400K)

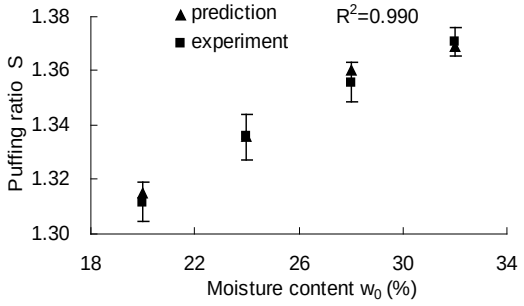

Fig. 3C (T_{sat}= 410K)

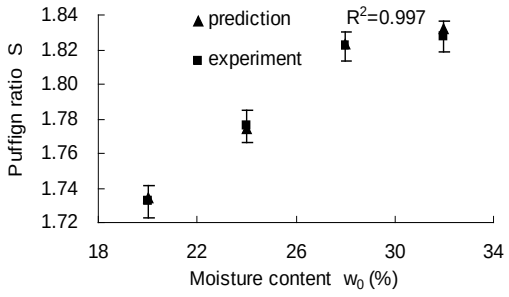

Fig. 3D (T_{sat}= 420K)

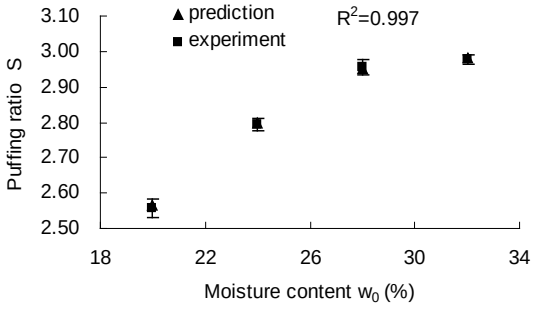

Fig. 3E (T_{sat}= 430K)

FIG. 3 EFFECT OF CARROT MOISTURE CONTENT ON PUFFING RATIO

Effect of Saturated Steam Temperature on Puffing Ratio

Carrots with moisture content (20, 24, 28, and 32%) were heated and puffed by saturated steam at different temperatures. Predicted puffing ratio values were obtained by Eq. (27). Predicted and experimental values are compared in Figures 4A–4D.

Predicted and experimental puffing ratio values were in agreement (R^2 >0.99) in carrots with 20–32% moisture content. Puffing ratios increased rapidly with increasing steam temperature from 390 to 430 K. Higher steam temperatures increase the heating capacity of the super-heated liquid and vapor pressure in the material. These

two positive factors result in more energy for puffing. Therefore, saturated steam temperature is a key factor for puffing.

Our previous studies have shown that the puffing ratio of carrot cubes initially increases with steam temperature. However, puffing ratio gradually decreases at steam temperatures >425 K (Song et al., 2010). On the other hand, the puffing ratio of banana slices increases from 410 to 430 K (An et al., 2010). This discrepancy in the results could be attributed to food shape. Carrot cubes have sharp angles where the puffing resistance is higher than that in the core. As a result, the core material is significantly destroyed by high energy, leading to uneven puffing. In spherical carrots and sliced bananas, the change of volume is correlated with the increase in diameter or thickness due to the uniform puffing resistance.

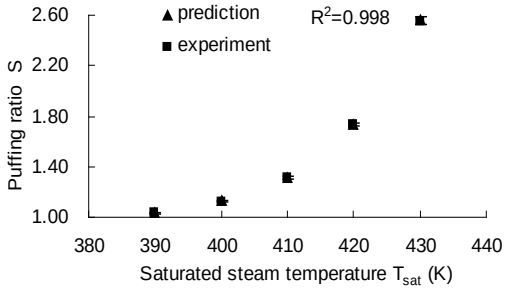

Fig. 4A (w_0= 20%)

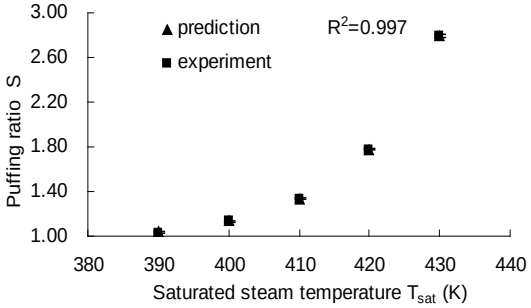

Fig. 4B (w_0= 24%)

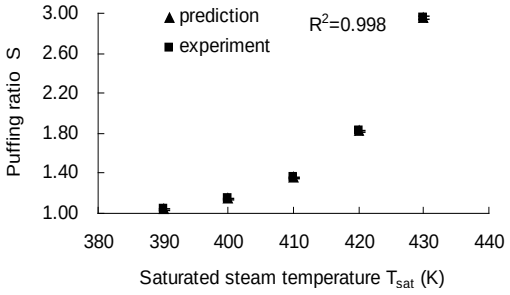

Fig. 4C (w_0= 28%)

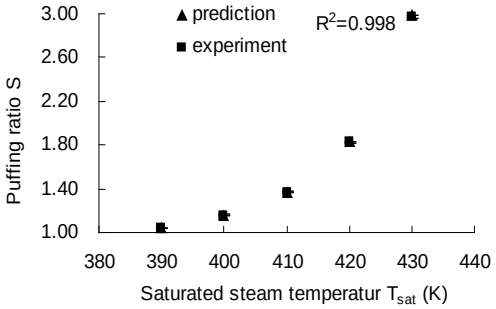

Fig. 4D (w_0= 32%)

FIG. 4 EFFECT OF SATURATED STEAM TEMPERATURE ON PUFFING RATIO

Conclusions

A power model of instant pressure drop with saturated steam-puffing of spherically-shaped carrots was generated following thermodynamic and elastic mechanic principles. The model revealed that puffing ratio was related to material shape, moisture content, mechanical property, saturated steam pressure, and saturated steam temperature. The model had high accuracy (R^2 >0.95) in predicting the effect of material moisture content and saturated temperature on puffing ratio. Superheated liquid in material flash evaporation and vapor in material instant release were important for puffing. The increase in material moisture content resulted in more condensed water during the heating process by saturated steam, which was beneficial to puffing. Saturated steam had higher pressure, which increased the heating capacity of the super-heated liquid and of the material vapor pressure, resulting in higher puffing ratios. Therefore, adequate material moisture content and saturated steam temperature (pressure) control puffing ratios.

ACKNOWLEDGMENTS

The authors express their gratitude to the Natural Science Foundation of China (project number: 31271913) and the Natural Science Foundation of Fujian Province (project number: 2011J01284) for their financial support.

REFERENCES

[1] Acevedo, N.C., Briones, V., Buera, P. and Aguilera, J.M. “Microstructure affects the rate of chemical, physical and color

changes during storage of dried apple discs". Journal of Food Engineering 85 (2008): 222-231.

[2] An F.P., Song H.B. and Song J.L. "Quality for super heated stream puffing and drying banana". Transactions of the Chinese Society for Agricultural Machinery 40, no. 12 (2010): 138-142.

[3] Burubai, W., Akor, A. J., Igoni, A. H. and Uyate, Y. T. "Effects of Temperature and Moisture Content on the Strength Properties of African Nutmeg (*Monodora Myristica*)". Bulgarian Journal of Agricultural Science 13 (2007): 703-712.

[4] Burubai, W., Amula, E., Davies, R.M., Etekpe, G.W.W. and Daworiye, S.P. "Determination of Poisson's ratio and elastic modulus of African nutmeg (*Monodora myristica*)". International Agrophysics 22 (2008): 99-102.

[5] Cen, H., Lu, R., Mendoza, F. and Beaudry, R.M. "Relationship of the optical absorption and scattering properties with mechanical and structural properties of apple tissue". Postharvest Biology and Technology 85 (2013): 30-38.

[6] Chen, S.N., Sun, J.H. and Wan, W. "Boiling liquid expanding vapor explosion: Experimental research in the evolution of the two-phase flow and over-pressure". Journal of hazardous materials 156, no. 1 (2008): 530-537.

[7] Dang, W.Y. and Liu, C.H. "Physical explosion calculation models of the pressurized gas vessels". Journal of Daqing Petroleum Institute 34, no. 2 (2010):104 -107.

[8] Datta, A.K. "Porous media approaches to studying simultaneous heat and mass transfer in food processes. I: Problem formulations". Journal of Food Engineering 80, no. 1 (2007): 80-95.

[9] Golacki, K. and Obroslak, R. "Determination of Poisson's ratio for carrot roots". Zeszyty Problemowe Postepow Nauk Rolniczych 451, no. 1 (1998): 221-227.

[10] Gong, Y.W., Lin, W.S., Gu., A.Z. and Lu, X.S. "A simplified model to predict the thermal response of PLG and its influence on BLEVE". Journal of hazardous materials 108, no. 1 (2004): 21-26.

[11] Hu, L.Y. and Zhang, L. "Flash evaporation of condensed water and flash evaporating condensed water". Energy Conservation, no. 1 (2006): 58-60.

[12] Huang, L.L., Zhang, M., Wang, L.P., Mujumdar, A.S. and Sun, D.F. "Influence of combination drying methods on composition, texture, aroma and microstructure of apple slices". LWT-Food Science and Technology 47 (2012): 183-188.

[13] Krokida, M.K. and Maroulis, Z.B. "Effect of microwave drying on some quality properties of dehydrated products". Drying Technology 17 (1999): 449-466.

[14] Lin, W.S., Gong, Y.W., Gao. T. and Gu, A.Z. "Experimental studies on the thermal stratification and its influence on BLEVEs". Experimental Thermal and Fluid Science 34, no. 7 (2010,): 972-978.

[15] Liu, J.Y. "Flash evaporation and application of condensed water". Energy Conservation Technology, no. 4 (1996): 2-3.

[16] Louka, N. and Allaf, K. "Expansion ratio and color improvement of dried vegetables texturized by a new process 'Controlled Sudden Decompression to the vacuum': Application to potatoes, carrots and onions". Journal of food engineering 65, no. 2 (2004): 233-243.

[17] Maghsoudi, H., Khoshtaghaza, M. H., Minaei, S. and Zaki Dizaji, H. "Fracture Resistance of Unsplit Pistachio (Pistacia vera L.) Nuts against Splitting Force, under Compressive Loading". Journal of Agricultural Science and Technology, no. 14 (2012): 299-310.

[18] Mayor, L., Moreira, R. and Sereno, A.M. "Shrinkage, density, porosity and shape changes during dehydration of pumpkin (Cucurbita pepo L.) fruits". Journal of Food Engineering 103 (2011): 29-37.

[19] Mostafa, K.D.K., Hossein, M. and Saeid, M. "Determination of poisson's ratio and young's modulus of red bean grains". Journal of Food Process Engineering 34 (2011): 1573-1583.

[20] Mounir, S., Halle, D. and Allaf K. "Characterization of pure cheese snacks and expanded granule powders textured by the instant controlled pressure drop (DIC) process". Dairy Science & Technology 91, no. 4 (2011): 441-455.

[21] Nath, A., Chattopadhyay, P.K. and Majumdar, G.C. "High temperature short time air puffed ready-to-eat (RTE) potato snacks: Process parameter optimization". Journal of food Engineering 2007, 80(3): 770-780.

[22] Niamnuy, C., Devahastin, S., Soponronnarit., S. and Vijaya Raghavan, G.S. "Modeling coupled transport phenomena and

mechanical deformation of shrimp during drying in a jet spouted bed dryer". Chemical Engineering Science 63, no. 22 (2008): 5503-5512.

[23] Nielsen, M., Martens, H.J. and Kaack. K. "Low frequency ultrasonics for texture measurements in carrots (Daucus carota L.) in relation to water loss and storage". Postharvest Biology and Technology 14 (1998): 297-308.

[24] Planas-Cuchi, E., Salla, J.M. and Casal, J. "Calculating overpressure from BLEVE explosions". Journal of Loss Prevention in the Process Industries 17 (2004): 431-436.

[25] Prugh, R.W. "Quantify BLEVE hazards". Chemical Engineering Progress 87, no. 2 (1991): 66-72.

[26] Rakesh, V. and Datta, A.K. "Microwave puffing: Determination of optimal conditions using a coupled multiphase porous media–Large deformation model". Journal of Food Engineering 107, no. 2 (2011): 152-163.

[27] Reid, R.C. "Possible mechanism for pressurized-liquid tank explosions or BLEVE's". Science 203, (1979): 1263-1265.

[28] Ressing, H,, Ressing, M. and Durance, T. "Modeling the mechanisms of dough puffing during vacuum microwave drying using the finite element method". Journal of Food Engineering 82, no. 4 (2007): 498-508.

[29] Rezzoug, S.A., Maache-Rezzoug, Z., Mazoyer, J., Jeannin M. and Allaf, K. "Effect of instantaneous controlled pressure drop process on the hydration capacity of scleroglucan: optimisation of operating conditions by response surface methodology". Carbohydrate Polymers 42, no. 1 (2000): 73-84.

[30] Sa-adchom, P., Swasdisevi, T., Nathakaranakule, A. And Soponronnarit, S. "Drying kinetics using superheated steam and quality attributes of dried pork slices for different thickness, seasoning and fibers distribution". Journal of Food Engineering 104 (2011): 105-113

[31] Sereno, A.M., Silva, M.A. and Mayor, L. "Determination of particle density and porosity in foods and porous materials with high moisture content". International Journal of Food Properties, no. 10 (2007): 455-469.

[32] Shmalko, M.E., Morawicki, R.O. and Ramallo, L.A. "Simultaneous determination of specific heat capacity and thermal conductivity using the finite-difference method". Journal of Food Engineering 31 (1996): 531-40.

[33] Shyu, S. L. and Hwang, L.H. "Effects of processing conditions on the quality of vacuum fried apple chips". Food Research International 34 (2001): 133-142.

[34] Song, H.B. and An, F.P. Optimization of super heated steam puffing drying technology for carrot. Transactions of the Chinese Society for Agricultural Machinery 41, no. 2 (2010): 127-131.

[35] Wang, Q. H., Dai, G. and Wang, D. F. "The analysis of the superheated liquid explosive energy and overpressure". Transactions of the Chemical Machinery 38, no. 3 (2011): 301-304.

[36] Xue, Q. Elasticity. Beijing, China: Beijing University Press, 2006.

[37] Yan, J.L. and Wang, Y.Q. Thermodynumics. 4th ed. Beijing, China: Higher Education Press, 2006: 243.

[38] Yan, Z., Sousa-gallagher, M.J. and Oliveira, F.A.R. "Shrinkage and porosity of banana, pineapple and mango slices during air-drying". Journal of Food Engineering 84 (2008): 430-440.

[39] Zhang, J., Datta, A.K. and Mukherjee, S. "Transport processes and large deformation during baking of bread". AIChE Journal 51, no. 9 (2005): 2569-2580.

Residue Dynamics and Safe Pre-Harvest Interval of Chlorpyrifos in Water Dropwort

Peng Qu[1], Minghao Piao[2], Jianguo Liu*[1], Jiakuan Xu[3]

[1]School of Environmental and Safety Engineering, Changzhou University, Changzhou 213164, China

[2]Mudanjiang branch of Heilongjiang Academy of Agricultural Sciences, Mudanjiang 157000, China

[3]Changzhou Station for Horticultural Technology Spread, Changzhou 213001, China

liujianguo@cczu.edu.cn

Abstract

Chlorpyrifos residue contents in market water dropwort, residue dynamics of chlorpyrifos and the safe pre-harvest interval (SPHI) in field water dropwort were conducted in Changzhou, Jiangsu Province, China. The results showed that concentrations of chlorpyrifos residues in more than half of the market samples (57%) exceeded the maximum allowable concentration (MAC, 0.05 mg kg^{-1}), according to the Chinese Standard (GB 2763 – 2014). The average chlorpyrifos content in the samples was 0.23 mg kg^{-1} that was 3.6 times higher than the MAC. Study on the residue dynamics of chlorpyrifos demonstrated that the half-life of chlorpyrifos residues in the water dropwort of early-sowing (in summer) and late-sowing (in autumn) were 4.1 and 5.4 days, respectively, and it took 31.2 and 43.1 days, respectively, for chlorpyrifos residues to decrease to the MAC level. In normal application dosage (recommended for vegetables), the SPHI was 30-35 days for the water dropwort of early-sowing, and 40 days for the water dropwort of late-sowing, which were much longer than the recommended pre-harvest interval (seven days) according to the Chinese Standard ((GB/T 8321 – 2000)). It may be the cause of high chlorpyrifos residue concentrations in market water dropwort.

Keywords

Chlorpyrifos; Water Dropwort [Oenanthe javanica (BL.) DC.]; Residues; Dynamics; Pre-harvest Interval; Pesticides

Introduction

In order to guarantee food supply for rapid increasing world population, pesticide application has been adopted to control pests in agricultural production worldwide for decades. It is estimated that about 45% of crop's yield is destroyed by pests and diseases in the world today. The utilization of pesticides controlled pests and increased the crop's yield initially, but the increasing use of chemical pesticides has caused environmental contamination and many adverse effects on human health simultaneously [1]. Pesticides are associated with many human health hazards, including acute harms (such as headaches and nausea) and chronic damages (such as cancer, endocrine disorder and reproductive impacts [2]. Therefore, the pesticide residue in food chain is a matter of public concern, especially in fresh fruits and vegetables [3].

In an evaluation on pesticide residues in fruits and vegetables of Xiamen, China, 17.2-18.9% of pakchoi cabbage, legume and leaf mustard samples exceeded the maximum allowable concentration (MAC) [4]. According to a monitoring program for pesticide residues in crops in Brazil, pesticide residues were found in 48.3% of the crop samples, and organophosphorus compounds were found in 30.8% of the samples. Chlorpyrifos was the organophosphorus pesticide mostly found (16.1% of the samples) [5].

Chlorpyrifos (O,O-diethyl O-3,5,6-trichloro-2-pyridyl phosphorothioate) is one of the most common organophosphate pesticides widely used in agriculture for protection of crops, such as vegetables, fruits and grains. It is one of the major pesticide residues detected in agricultural products [6, 7]. It is toxic to central and peripheral nervous systems, which may cause lethal or sub-lethal effects on human body. It can also interfere with the development of nervous system while exposure in pregnant stage [8]. Some studies showed that there were some associations between chlorpyrifos exposure and lung and prostate cancer [9, 10]. Therefore, environmental behavior, biodegradation and toxic effects of chlorpyrifos has attracted much attention [11, 12]. Water dropwort

2327-7246/15/02 058-6 © 2015 DEStech Publications, Inc.
doi:10.12783/ijast.2015.0302.04

(*Oenanthe javanica*) is one of the most popular vegetables and widely cultivated in China and Southeast Asia. Study on the residue dynamics of pesticides is recognized as an important initiative to reduce their threat on human health. However, the residue dynamics of chlorpyrifos in water dropwort are not clear at present.

Materials and Methods

Field Experimental Design

The research was carried out in Changzhou, Jiangsu Province, China (30° 41' N, 119° 50' E). The field experiments were designed as split-plots measuring 200 m^2 each in three replicates, according to the "Guideline on Pesticide Residue Trials" of China (NY/T 788 – 2004). The plots were separated by irrigation channels. Water dropwort was sowed at two times, e.g. August 12 (early-sowing) and October 5 (late-sowing). In residue dynamics experiment, chlorpyrifos was applied at August 27 for early-sowing and October 20 for late-sowing. In the experiment of safe pre-harvest interval (SPHI), chlorpyrifos was applied at 10, 15, 20, 25, 30, 35, 40, 45 days before harvest day. Chlorpyrifos (EC, 48% w/v) was dissolved in water and sprayed at the recommended dosage of 360 g a.i. ha^{-1} for vegetables. For control treatment, no pesticide was sprayed.

Sampling and Analytical Procedures

Twenty-one market samples were collected from seven vegetable markets in Changzhou, China. For the study of residue dynamics, the field samples were collected from the plots at 0.125 (three hours), 1, 3, 7, 13, 20, 30, 45 and 60 days after the application of chlorpyrifos, respectively. For the experiment of SPHI, the field samples were collected from the plots at the harvest time. The samples were transported to the laboratory at 4 ℃ and in darkness in labeled polyethylene bags, and were processed promptly and stored at -20 °C until analysis. Extraction and clean up procedures of chlorpyrifos residues from the samples were carried out as described by Chen et al. [13]. Concentrations of chlorpyrifos were tested with Agilent 6890N gas chromatograph equipped with a flame photometric detector (FPD) and a DB-17 (30 m length, 0.25 μm film thickness, 0.53 mm i.d.) capillary column. The gas chromatographic analysis was performed under the conditions described by Chen et al. [13].

Quality Control of Analytical Procedures

Chlorpyrifos standards (99.5% of purity) were obtained from the Institute for the Control of Agrochemicals, Ministry of Agriculture (ICAMA), China. A stock solution of chlorpyrifos was prepared at 100 mg kg^{-1} in acetonitrile in a volumetric flask and conducted at 4 ℃ before being used. Recoveries experiments were conducted to confirm the validity of the methods. Different known concentrations of chlorpyrifos (0.01, 0.02, 0.1, 0.2, 0.5 and 1 mg L^{-1}) were prepared by diluting the stock solution with acetonitrile.

Quality control was carried out using duplicate samples (every 20 samples), spiked samples (one per process batch), repeat samples (one per batch), and reagent blank sample (one deionized water per batch). The spiked samples were analyzed before and during the analysis of all batches of the samples.

Results and Discussion

The contents of chlorpyrifos residues in twenty-one market samples were shown in Figure 1. Chlorpyrifos concentrations in the samples ranged from 0.02 mg kg^{-1} to 1.09 mg kg^{-1} (54.5-fold variation). The average chlorpyrifos contents in the samples was 0.23 mg kg^{-1} that was 4.6 times of the maximum allowable concentration (MAC, 0.05 mg kg^{-1}) for chlorpyrifos in water dropwort, according the Chinese Standard (GB 2763 – 2014). In twenty-one samples, twelve samples (57%) showed chlorpyrifos concentrations above the MAC. Vegetables and fruits showing pesticide concentrations above the MAC were also found in other countries. In Poland, fifteen different pesticides were detected in 32% vegetable samples, and 9% samples exceeded the MAC. Chlorpyrifos was one of the most commonly detected pesticides, and it presented in 27.4% samples [14]. According to a survey in Nordic countries (Denmark, Finland, Norway and Sweden) on the presence of pesticide residues in the fruits and vegetables imported from Southeast Asia, the contents of pesticide residues were above the MAC in 12% of the samples. Some of the products were assessed to represent possible acute health risk for consumers. Chlorpyrifos

was one of the most frequently detected pesticides [15]. Water dropwort is one of the most popular vegetables and widely cultivated in China and Southeast Asia, for its good taste and abundant nutrients (protein, Ca, P, Fe, etc.) [16]. Therefore, chlorpyrifos residue in market water dropwort is a great threat to human health in the countries.

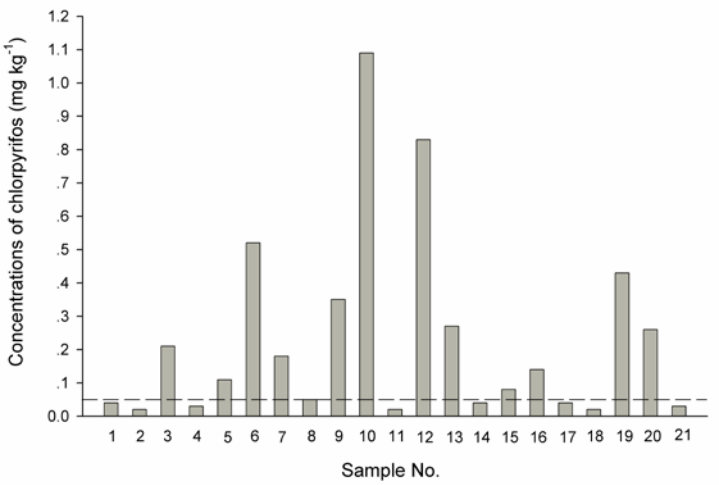

FIGURE 1. CHLORPYRIFOS CONCENTRATIONS IN THE MARKET SAMPLES OF WATER DROPWORT IN CHANGZHOU, JIANGSU PROVINCE, CHINA
THE MAXIMUM ALLOWABLE CONCENTRATION (MAC, 0.05 MG KG^{-1}) FOR CHLORPYRIFOS IN WATER DROPWORT, ACCORDING THE CHINESE STANDARD (GB 2763 – 2014).

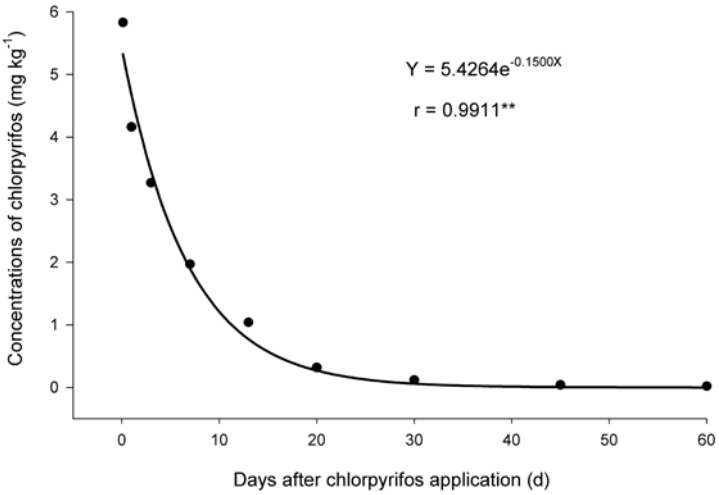

FIGURE 2. RESIDUE DYNAMICS OF CHLORPYRIFOS IN THE WATER DROPWORT OF EARLY-SOWING (ON AUGUST 12)
R CORRELATION COEFFICIENT, ** SIGNIFICANT AT $P_{0.01}$ LEVEL

The residue dynamics of chlorpyrifos in the water dropwort of early-sowing is displayed in Figure 2. According to the dynamic equation, the half-life of Chlorpyrifos residue in the water dropwort was 4.1 days, and the concentration of chlorpyrifos residues will decrease to the MAC (0.05 mg kg^{-1}) in 31.2 days after chlorpyrifos application. The residue dynamics of chlorpyrifos in the water dropwort of late-sowing are shown in Figure 3. Calculated from the dynamic equation, the half-life of Chlorpyrifos in the water dropwort was 5.4 days, and the concentrations of chlorpyrifos residues will decrease to the MAC in 43.1 days after chlorpyrifos application.

Degradation of chlorpyrifos in plants, soils and water are a very complicated process, and influenced by many factors, such as plant species, climates, soil properties, application rates, etc [17]. The half-life time and the time of decreasing to the MAC for the water dropwort of late-sowing (in autumn) were much longer than those for the water dropwort of early-sowing (in summer). The reasons may be in two aspects: (1) higher atmospheric temperature in the growing season for early-sowing water dropwort than for late-sowing water dropwort resulted in faster degradation and evaporation of chlorpyrifos in the water dropwort of early-sowing than in the water dropwort of late-sowing; (2) higher atmospheric temperature will result in faster growth of plants and greater dilution effect in chlorpyrifos concentrations for early-sowing water dropwort versus late-sowing water dropwort.

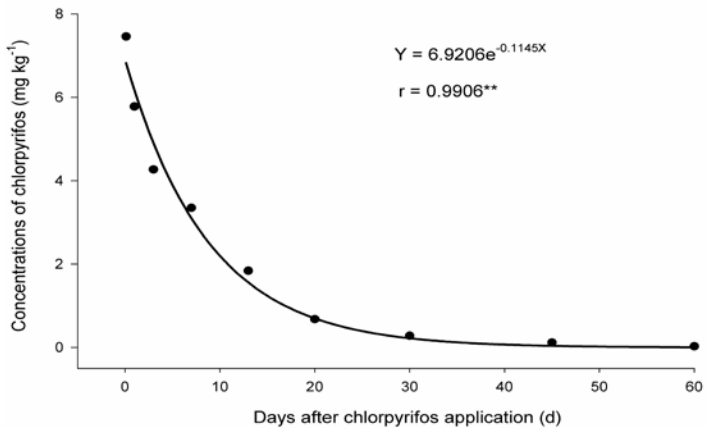

FIGURE 3. RESIDUE DYNAMICS OF CHLORPYRIFOS IN THE WATER DROPWORT OF LATE-SOWING (ON OCTOBER 5)
R CORRELATION COEFFICIENT, ** SIGNIFICANT AT $P_{0.01}$ LEVEL

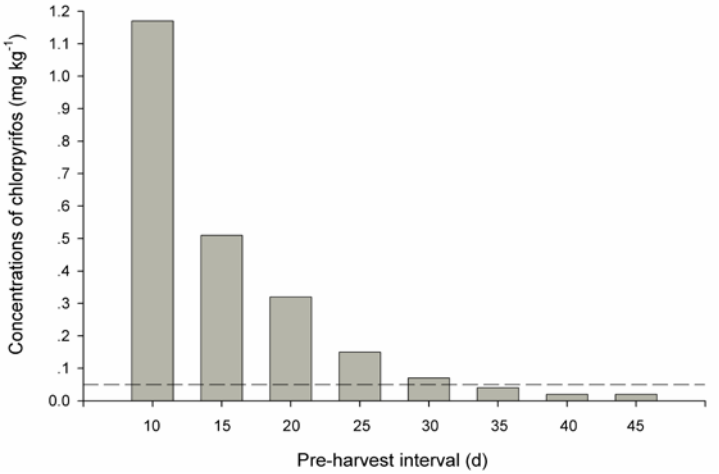

FIGURE 4. CONCENTRATIONS OF CHLORPYRIFOS RESIDUES IN THE WATER DROPWORT OF EARLY-SOWING FOR DIFFERENT PRE-HARVEST INTERVALS

It was reported that the contents of pesticide residues in harvested crops were much related to times and dosages of the chemical treatments, specifically at the mid- and late-stages of the crops [18]. Present study on safe pre-harvest interval (SPHI) of chlorpyrifos application in water dropwort presented that the SPHI was 30-35 days for the water dropwort of early-sowing (Figure 4), and 40 days for the water dropwort of late-sowing (Figure 5). According to the Guideline for Safety Application of Pesticides in China (GB/T 8321 – 2000), the recommended pre-harvest interval for the application of pesticides in vegetables is only seven days, which is much shorter than the SPHI in the present study.

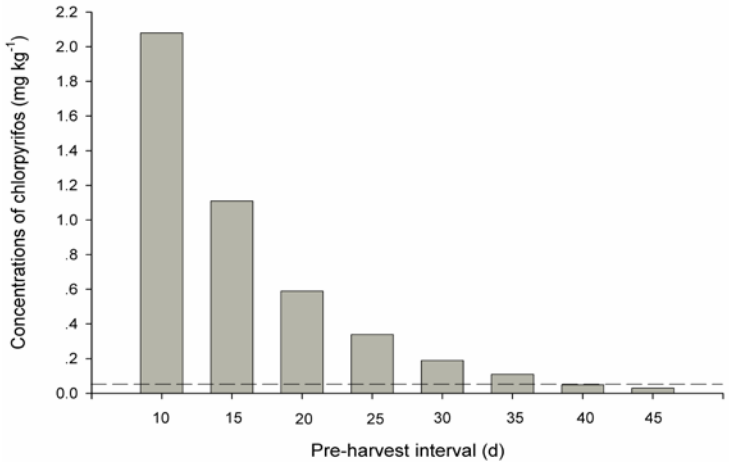

FIGURE 5. CONCENTRATIONS OF CHLORPYRIFOS RESIDUES IN THE WATER DROPWORT OF LATE-SOWING FOR DIFFERENT PRE-HARVEST INTERVALS

Due to the poor management and inadequate regulation on chemical applications, the cases of pesticide poisonings and food contaminations are far more in developing countries than in developed countries [19,20]. In Aegean region of Turkey, 8.4% of fruit samples and 9.8% of vegetable samples contained pesticide residues above the MAC. Chlorpyriphos was one of the most detected pesticide residues [21].

Therefore, the residue dynamics and the SPHI of the chemicals applied in vegetable production need much more concerns and studies.

Conclusion

Water dropwort is one of the most popular and widely cultivated vegetables in China and Southeast Asia, and chlorpyrifos is one of the most frequently used pesticides in vegetable production worldwide. Chlorpyrifos residues above the maximum allowable concentration (MAC, 0.05 mg kg^{-1}) in water dropwort may be a threat to human health. In the present study, the concentrations of chlorpyrifos residues exceeded the MAC in more than half of the market water dropwort samples (57%). The average chlorpyrifos contents in the samples was 3.6 times higher than the MAC. In the water dropwort of early-sowing (in summer) and late-sowing (in autumn), the half-life of chlorpyrifos residues were 4.1 and 5.4 days, respectively, and it took 31.2 and 43.1 days, respectively, for chlorpyrifos residues to decrease to the MAC. In normal application dosage (recommended for vegetables), the safe pre-harvest interval (SPHI) for the water dropwort of early-sowing and late-sowing was 30-35 and 40 days, respectively, which were much longer than the recommended pre-harvest interval (seven days) in China. Perhaps it is the cause of high concentrations of chlorpyrifos residues in market water dropwort.

ACKNOWLEDGMENTS

This study was funded by the National Natural Science Foundation of China (31071350) and the Agricultural "Three Projects" of Changzhou.

REFERENCES

[1] Bhanti, M., Taneja, A. 2007. "Contamination of vegetables of different seasons with organophosphorous pesticides and related health risk assessment in northern India." Chemosphere, 69, 63–68.

[2] Berrada, H., Fernández, M., Ruiz, M. J., Moltó, J. C., Mañes, J., Font, G. 2010. "Surveillance of pesticide residues in fruits from Valencia during twenty months (2004/05)." Food Control, 21, 36–44.

[3] Solecki, R., Davies, L., Dellarco, V., Dewhurst, I., Raaij, M. V., Tritscher, A. 2005. "Guidance on setting of acute reference dose (ARfD) for pesticides." Food and Chemical Toxicology, 43, 1569–1593.

[4] Chen, C., Qian, Y. Z., Chen, Q., Tao, C. J, Li, C. Y, Li, Y. 2011. "Evaluation of pesticide residues in fruits and vegetables from Xiamen, China." Food Control, 22, 1114–1120.

[5] Jardim, A. N. O., Caldas, E. D. 2012. "Brazilian monitoring programs for pesticide residues in food – Results from 2001 to 2010." Food Control, 25, 607–616.

[6] Sun, F., Chen, H. S. 2008. "Monitoring of pesticide chlorpyrifos residue in farmed fish: Investigation of possible sources." Chemosphere, 71, 1866–1869.

[7] Phung, D. T., Connell, D., Miller, G., Hodge, M., Patel, R., Cheng, R. et al. 2012. "Biological monitoring of chlorpyrifos exposure to rice farmers in Vietnam." Chemosphere, 87, 294–300.

[8] Slotkin, T. A., Levin, E. D., Seidler, F. J. 2006. "Comparative development neurotoxicity of organophosphate insecticides: effects on brain development are separable from systematic toxicity." Environmental Health Perspectives, 114, 746–751.

[9] Alavanja, C. R., Samanic, C., Dosemecil, M., Lubin, J., Tarone, R., Lynch, C.F., et al. 2003. "Use of agricultural pesticides and prostate cancer risk in the agricultural health study cohort." American Journal of Epidemiology, 157, 800–814.

[10] Lee, W. J., Blair, A., Hoppin, J. A., Rusiecki, J. A., Sandler, D. P., Dosemeci, M., et al. 2004. "Cancer incidence among pesticide applicators exposed to chlorpyrifos in the agricultural health study." Journal of the National Cancer Institute, 96, 457–465.

[11] Singh, B. K., Walker, A., Wright, D. J. 2006. "Bioremedial potential of fenamiphos and chlorpyrifos degrading isolates: influence of different environmental conditions." Soil Biology & Biochemistry, 38, 2682–2693.

[12] Fang, H., Yu, Y., Chu, X., Wang, X., Yang, X., Yu, J. 2009. "Degradation of chlorpyrifos in laboratory soil and its impact on soil microbial functional diversity." Joural Environmental Sciences, 21, 380–386.

[13] Chen, C., Qian, Y. Z., Liu, X. J., Tao, C. J, Liang, Y., Li, Y. 2012. "Risk assessment of chlorpyrifos on rice and cabbage in China." Regulatory Toxicology and Pharmacology, 62, 125–130

[14] Qozowicka, B., Jankowska, M., Kaczyński, P. 2012. "Pesticide residues in Brassica vegetables and exposure assessment of consumers." Food Control, 25, 561–575.

[15] Skretteberg, L. G., Lyrån, B., Holen, B., Jansson, A., Fohgelberg, P., Siivinen, K. et al. 2015. "Pesticide residues in food of plant origin from Southeast Asia - A Nordic project." Food Control, 51, 225–235.

[16] Liu, G. R., Liu, Y. L. 2007. "Growth characteristics and cultivation technologies of water dropwort." Shanghai Vegetables, 4, 34–36. (in Chinese)

[17] Zhang, X., Shen, Y., Yu X. Y., Liu X. J. 2012. "Dissipation of chlorpyrifos and residue analysis in rice, soil and water under paddy field conditions." Ecotoxicology and Environmental Safety, 78, 276–280.

[18] Zhang, C. Z., Zhang, X. M., Tian Z. H., He D. J., Liu X. J. 2010. "Degradation of chlorpyrifos and fipronil in rice from farm to fork and risk assessment." Agricultural Sciences in China, 9, 754–763.

[19] Bhanti, M., Shukla, G., Taneja, A. 2004. "Contamination levels of organochlorine pesticides and farmers' knowledge, perception, practices in rural India: a case study." Bulletin of Environmental Contamination and Toxicology, 73, 787–793.

[20] Waichman, A. A., Eve, E., Nina, N. C. S. 2007. "Do farmers understand the information displayed on pesticide product labels? A key question to reduce pesticides exposure and risk of poisoning in the Brazilian Amazon." Crop Protection, 26, 576–583.

[21] Bakırcı, G. T., Acay, D. B. Y., Bakırcı, F., & Ötleş, S. 2014. "Pesticide residues in fruits and vegetables from the Aegean region, Turkey." Food Chemistry, 160, 379–392.